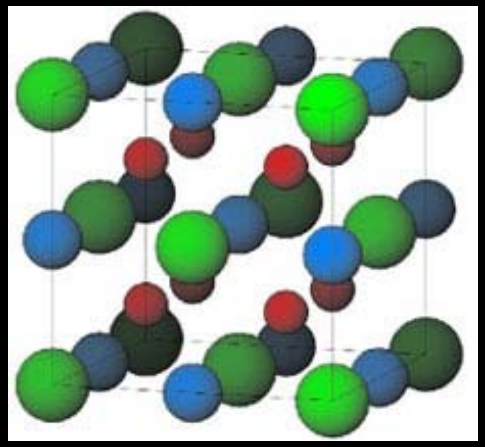

$$G = G_0 + G_0 V G$$

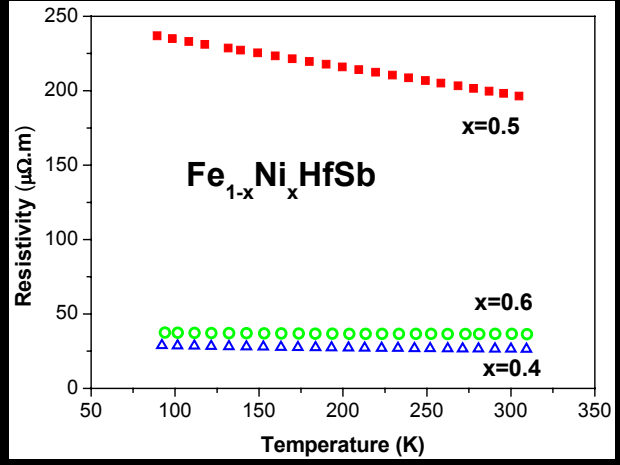

Jak z metali powstaje półprzewodnik ?

od równań rozpraszania wielokrotnego
do elektronowych diagramów fazowych

Janusz Toboła

Faculty of Physics and Applied Computer Science,
AGH University of Science and Technology, Krakow, Poland

Plan

Podział ciał stałych od strony struktury elektronowej (INS, SC, M, HFM, DMS)

Koncepcja elektronowych diagramów fazowych (przykłady).

Metody elektrodynamiki kwantowej (równania MST - Multiple Scattering Theory)

Technika Korringa-Kohn-Rostoker (KKR) obliczeń struktury elektronowej ciał stałych

Nowe ujęcie metody KKR (quasi-linear form) i korzyści przy obliczeniach wieloatomowych układów złożonych.

W stronę układów realnych - coherent potential approximation (CPA)

Własności fizyczne uzyskiwane z obliczeń (magnetyczne, transportowe. termoelektryczne, magnetokaloryczne, nadprzewodzące)

Wyniki poszukiwań teoretycznych (stopy pół-Heuslera, skutterudyty, fazy Chevrela),

Półprzewodnik poprzez stapianie metali (obliczenia) i powierzchnia Fermiego.

Pomiary transportowe (przewodnictwo, siła termoelektryczna) i „czworobok" TE.

W stronę spintroniki – magnetyczne półprzewodniki na bazie pół-Heuslerów ?

Współpraca

Search for new materials requires understanding of „old" systems

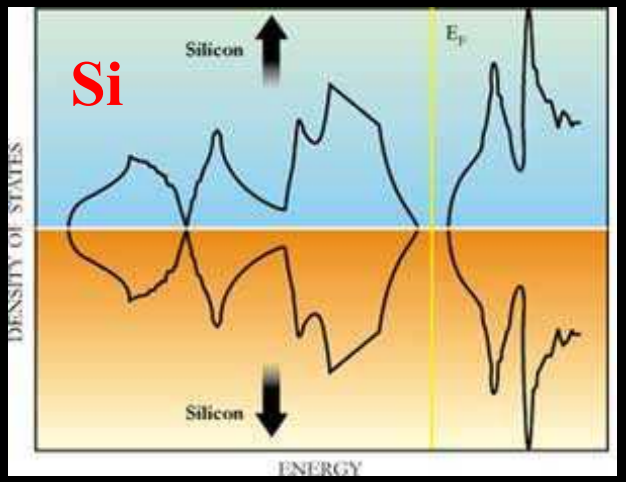

Semiconductor

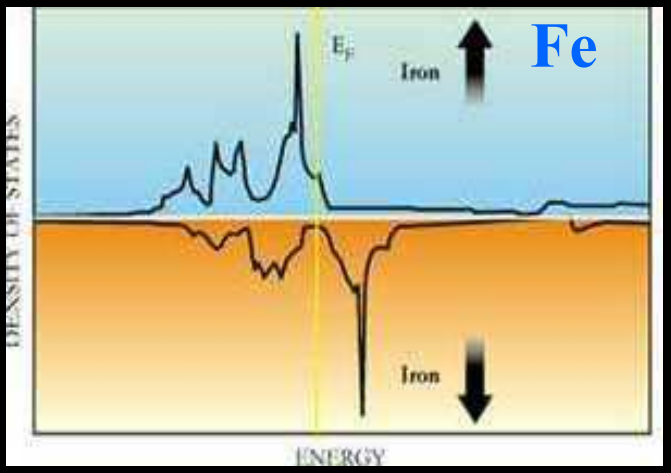

Metallic ferromagnet

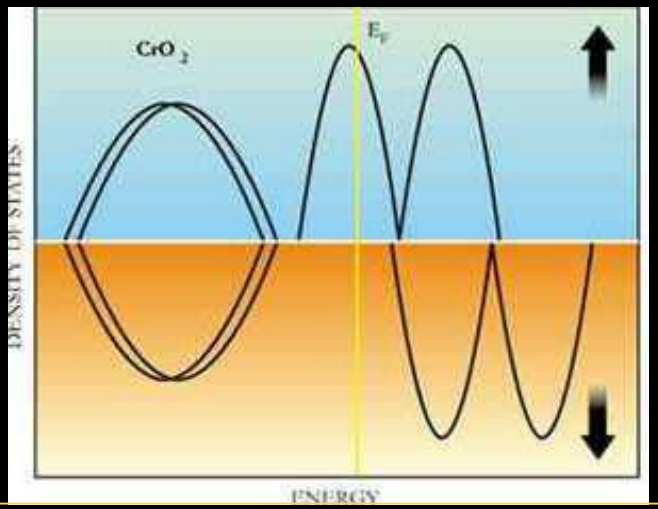

Half-metallic ferromagnet

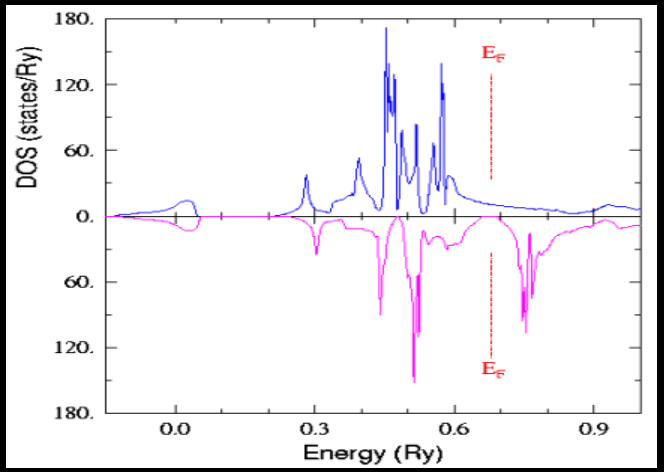

Magnetic semiconductor ??

Unusual properties of half-metals

-Predicted theoretically by band structure calculations

-(de Groot et al., PRL 1983)

-lack of Fermi surface for one spin-direction (positron

-anihilation experiments (Mijnarends, 1986),

- integer value of magnetic moment per WS cell,

- uncommon electron transport behaviours

(lack of spin-flip term in conductivity),

- giant magneto-optical Kerr effect

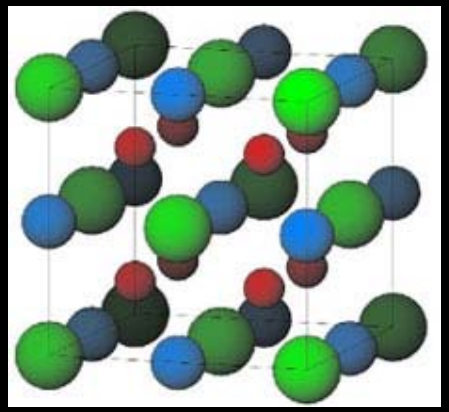

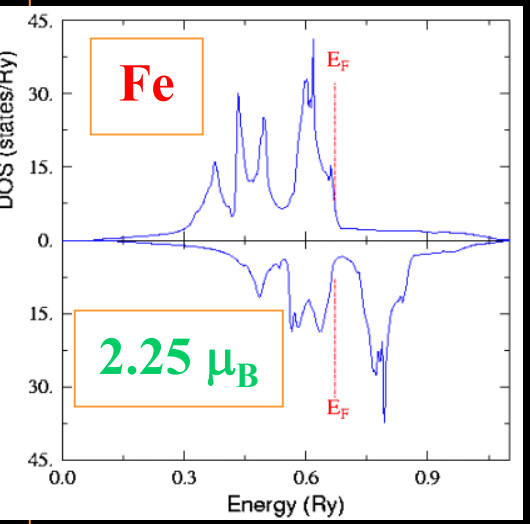

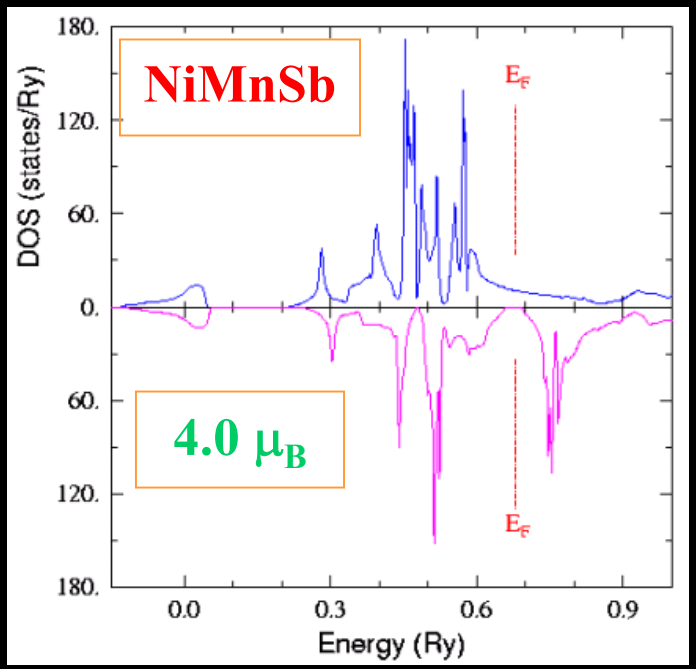

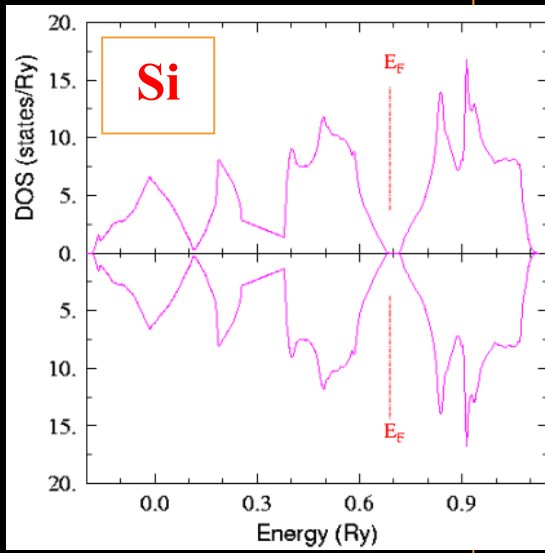

Heusler phases X_2YZ, XYZ (1903)

DO_3 structure

Fm3m (typ Fe_3Al)

X : (0,0,0), (1/2,1/2,1/2)

X : (3/4,3/4,3/4)

Z: (1/4,1/4,1/4)

Normal Heusler $L2_1$

Fm3m (typ Cu_2MnAl)

X : (0,0,0), (1/2,1/2,1/2)

Y : (3/4,3/4,3/4)

Z: (1/4,1/4,1/4)

Half-Heusler $C1_b$

F-43m (typ AgMgAs)

X :	(0,0,0)	4a
Y :	(3/4,3/4,3/4)	4d
Z:	(1/4,1/4,1/4)	4c

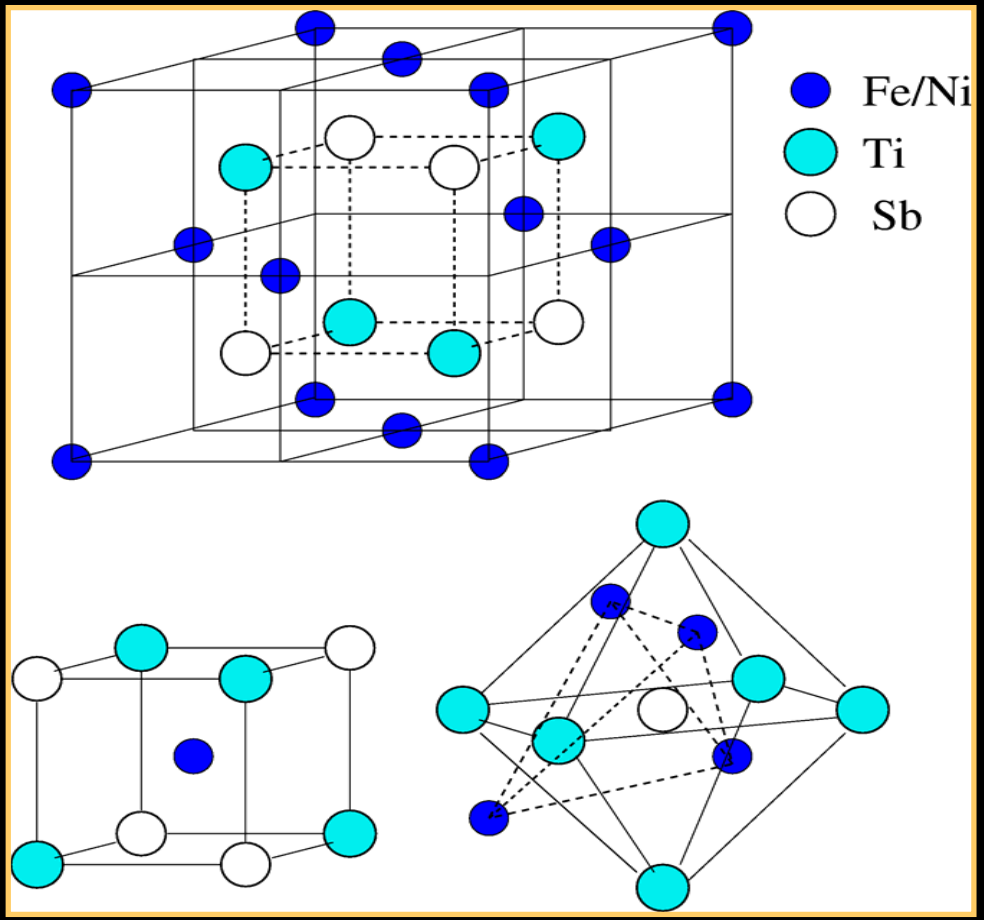

Crystal stability

***sp^3, d* orbitals**

„True" Heusler system $Co_{2-x}Fe_xMnSi$

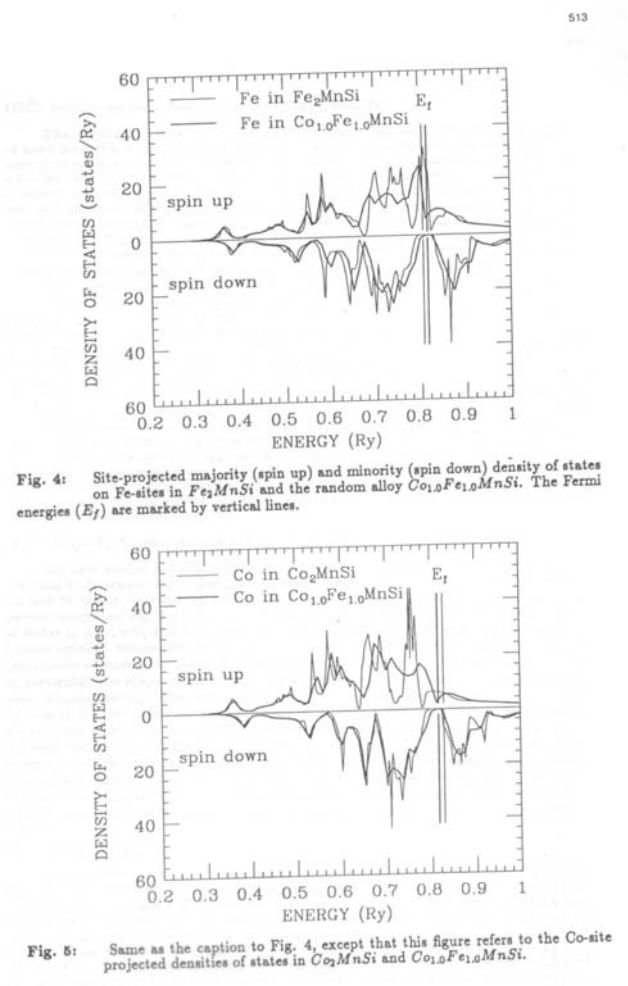

Fig. 4: Site-projected majority (spin up) and minority (spin down) density of states on Fe-sites in Fe_2MnSi and the random alloy $Co_{1.0}Fe_{1.0}MnSi$. The Fermi energies (E_f) are marked by vertical lines.

Fig. 5: Same as the caption to Fig. 4, except that this figure refers to the Co-site projected densities of states in Co_2MnSi and $Co_{1.0}Fe_{1.0}MnSi$.

Density of states

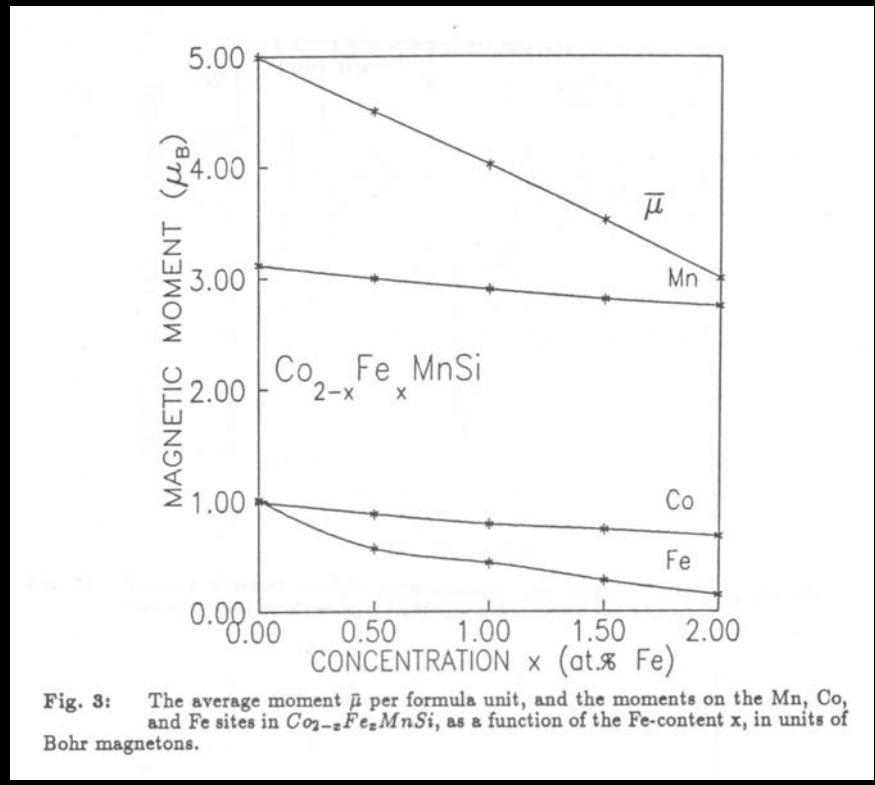

Fig. 3: The average moment $\bar{\mu}$ per formula unit, and the moments on the Mn, Co, and Fe sites in $Co_{2-z}Fe_zMnSi$, as a function of the Fe-content x, in units of Bohr magnetons.

Magnetic moment vs. concentration

Bansil, Kaprzyk, Tobola, MRS Symp. Proc. 253 (1992)

Structural relations

half-Heusler

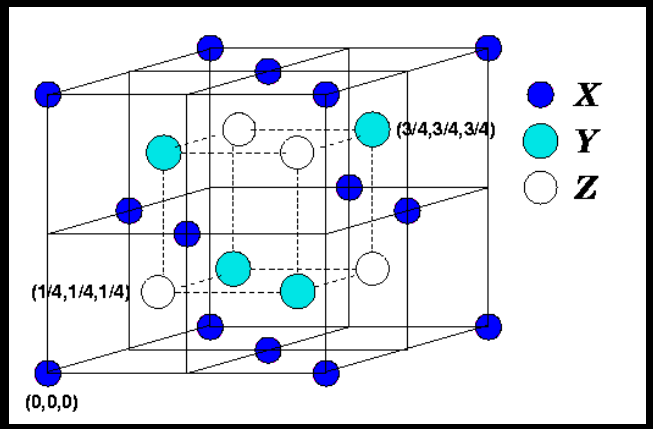

Zinc blende

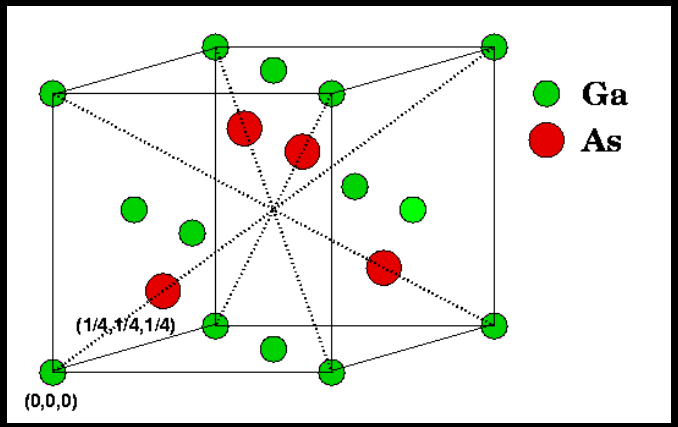

DOS of $Cd_{1-x}Mn_xTe$

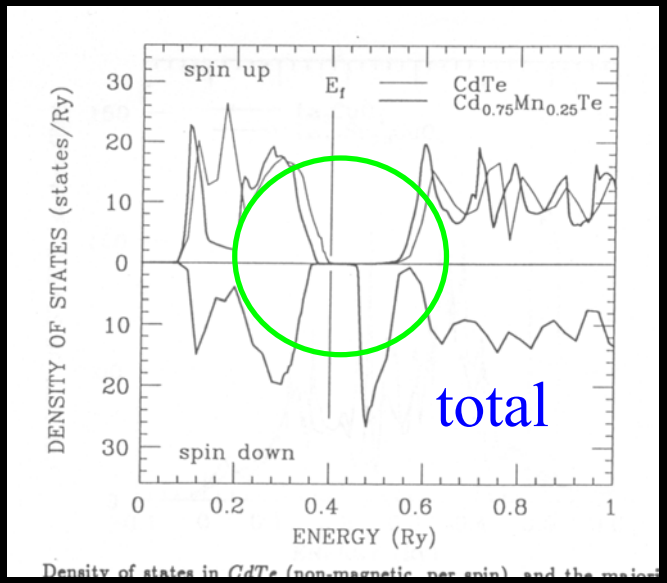

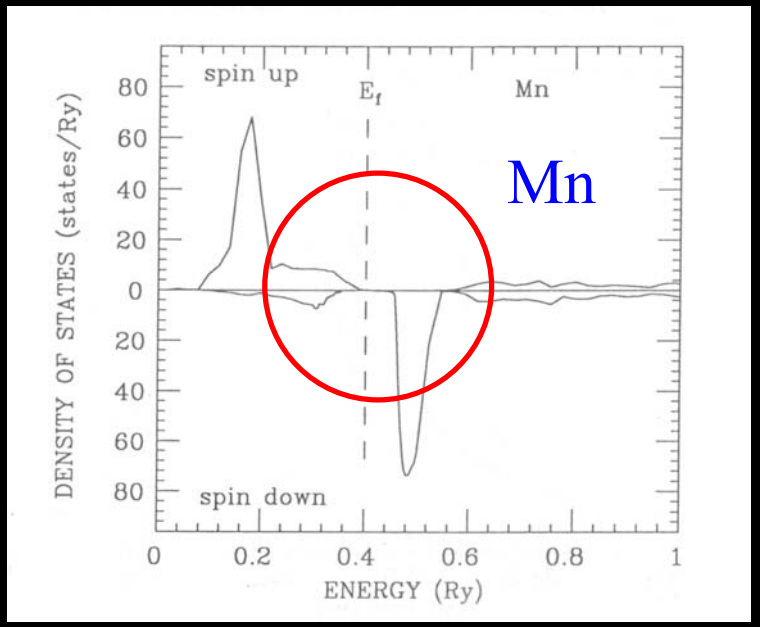

Elektronowy diagram fazowy układów pół-Heuslera

Toboła et al.., JMMM (1996), J. Phys. CM (1998), J.All.Comp. (2000)

Oporność właściwa

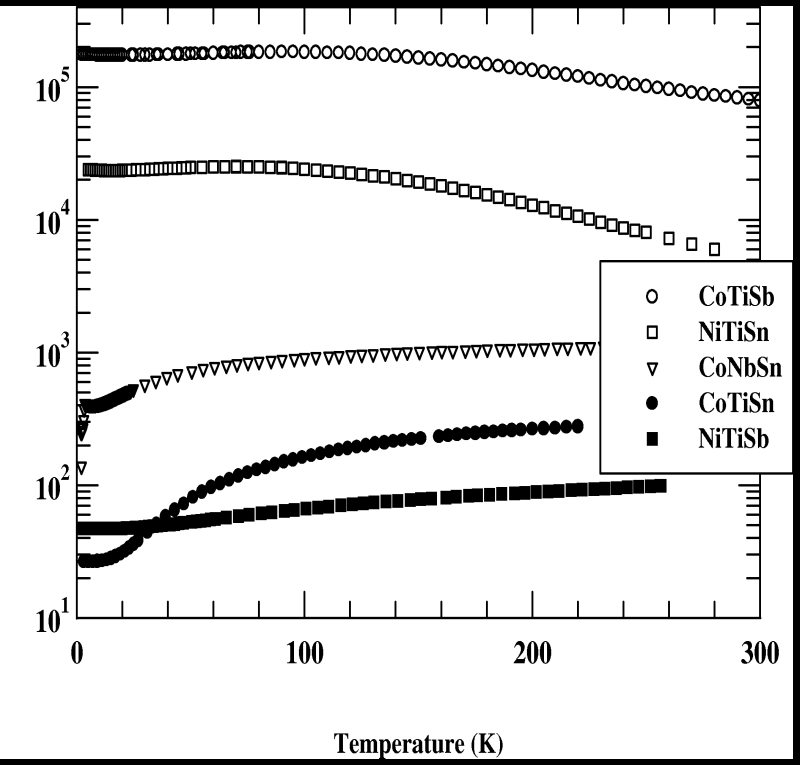

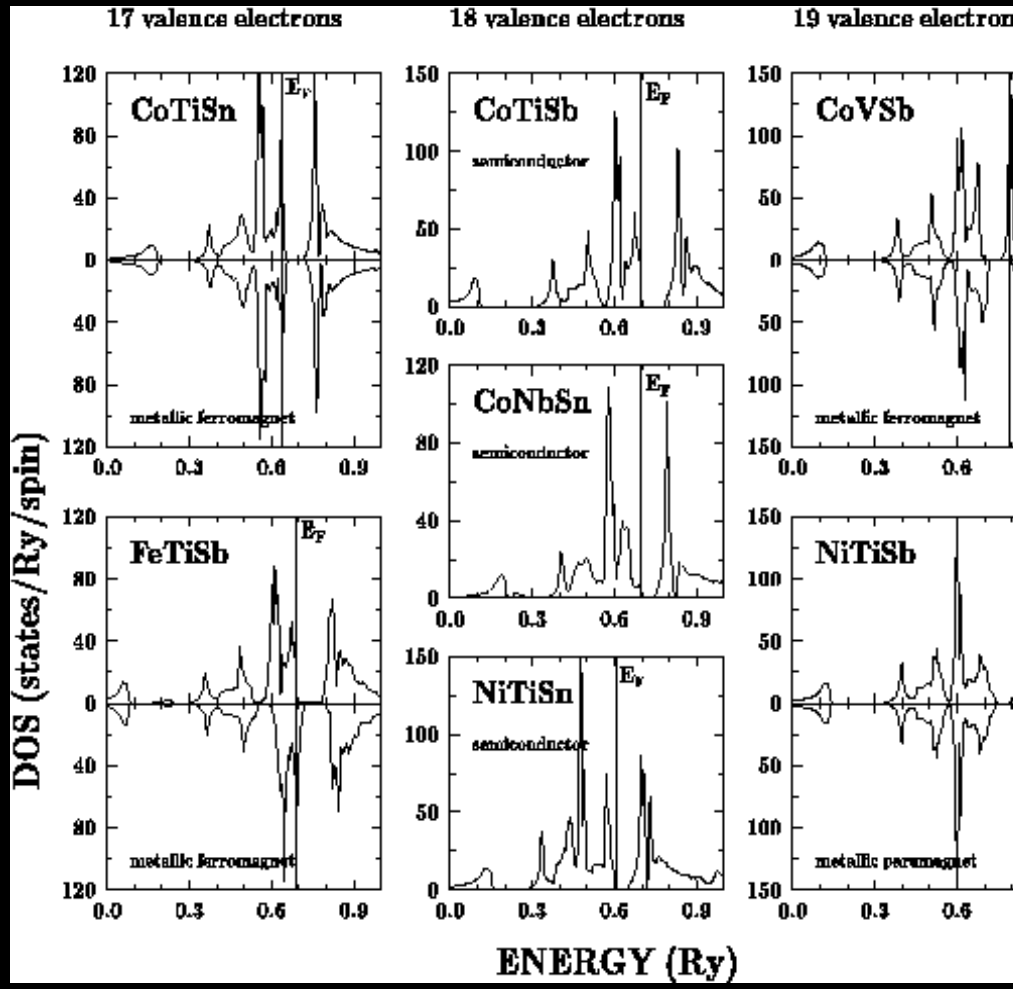

CoTiSn

^{27}Co : ^{18}Ar 4 s^2 3 d^7 (9)

^{22}Ti : ^{18}Ar 4 s^2 3 d^2 (4)

^{50}Sn:[^{36}Kr4d^{10}] 5s^{2}5p^2 (4)

FeVSb

^{26}Fe: ^{18}Ar 4 s^2 3 d^6 (8)

^{23}V : ^{18}Ar 4 s^2 3 d^3 (5)

^{51}Sb:[^{36}Kr4d^{10}] 5s^{2}5p^3 (5)

NiMnSb

^{28}Ni: ^{18}Ar 4 s^2 3 d^8 (10)

^{25}Mn: ^{18}Ar 4 s^2 3 d^5 (7)

^{51}Sb:[^{36}Kr4d^{10}] 5s^{2}5p^3 (5)

Własności „na życzenie”?

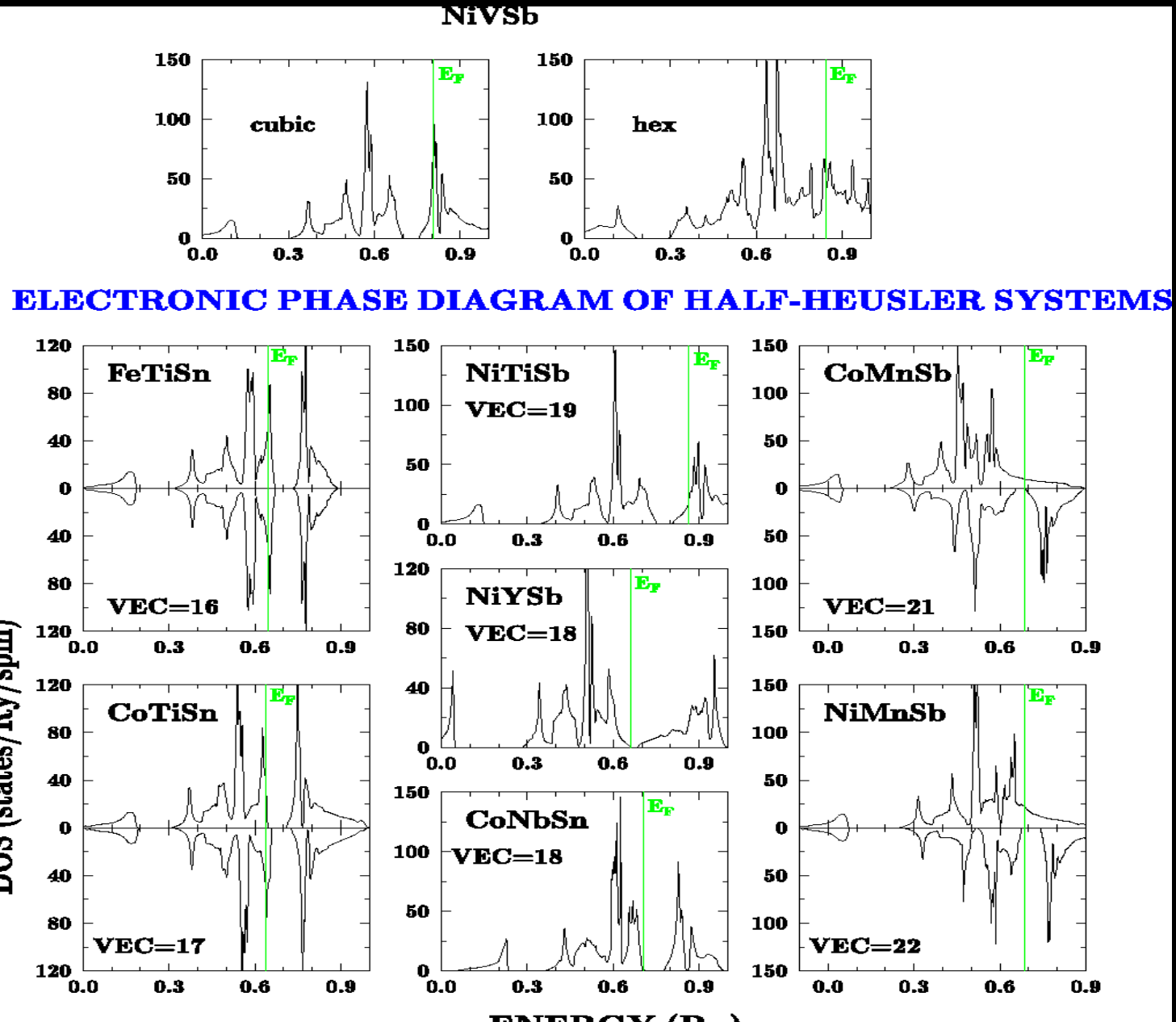

Prognozowanie przejść :

FM-PM

FM-HMF

FM-SC

PM-SC

PM-SC-PM

FM-SC-PM

Strukturalna niestabilność

NiVSb, CoCrSb, ... **VEC=20**

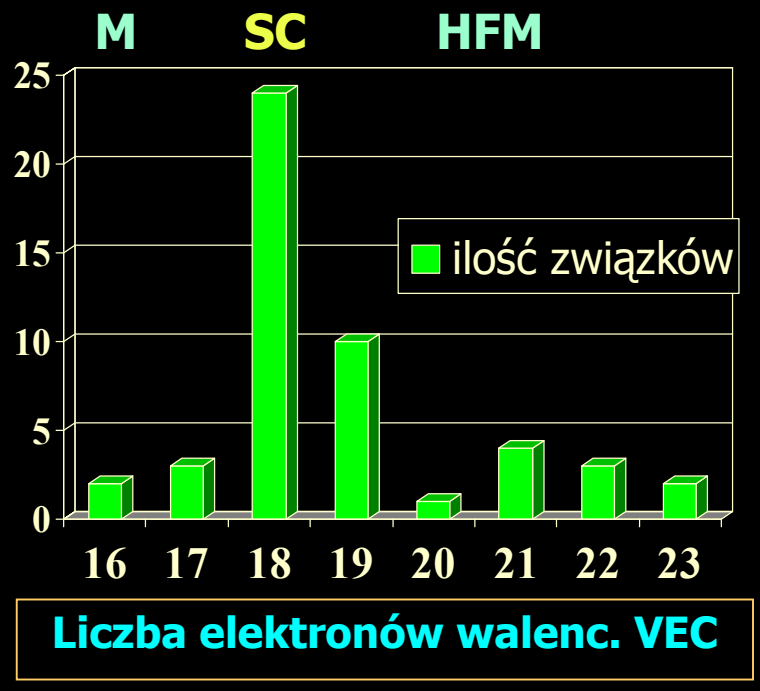

eksperyment	teoria
synteza struktury	w strukturze $C1_b$
$C1_b$ nie udaje się	1.5 μ_B / atom V !!

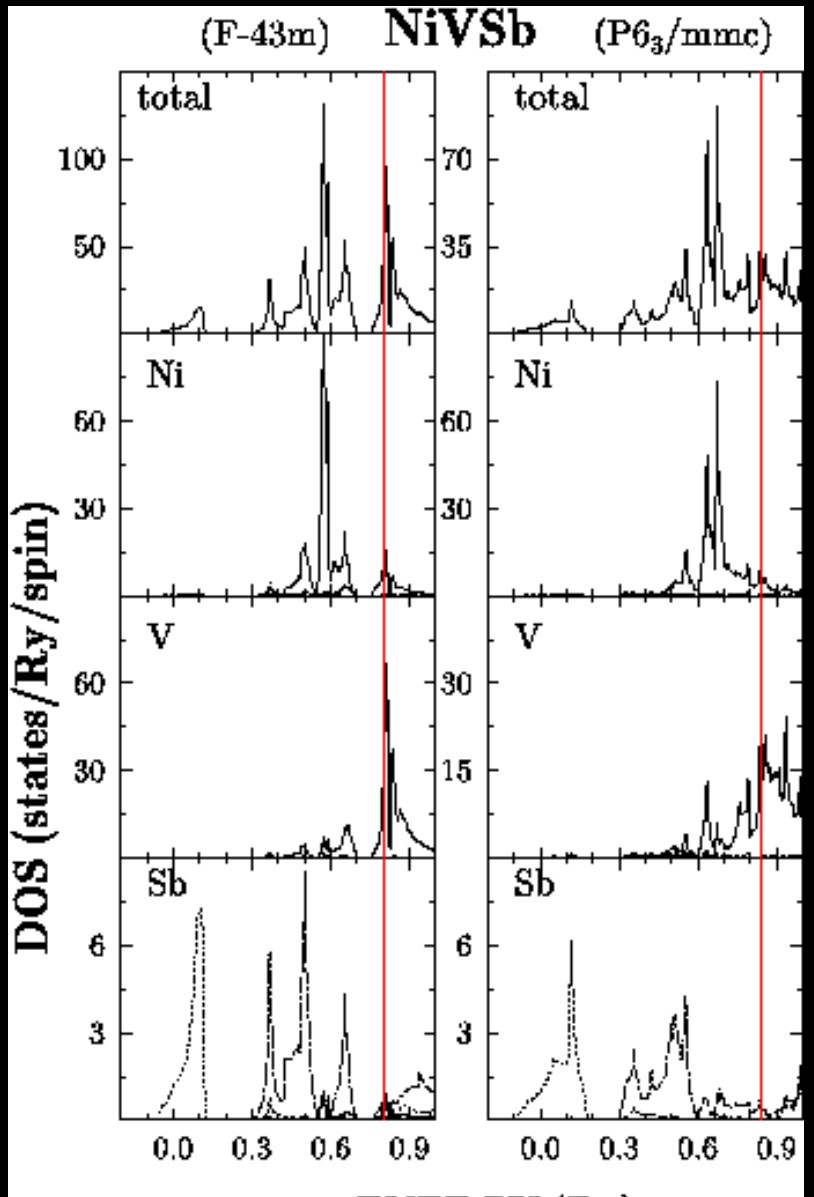

Multiple Scattering Theory (1)

$$G = G_0 + G_0 V G.$$

Dyson equations

Crystal potential

$$V = \sum_i v_i.$$

$$G_0 = \frac{1}{E - H}$$

Free-electron
Green function

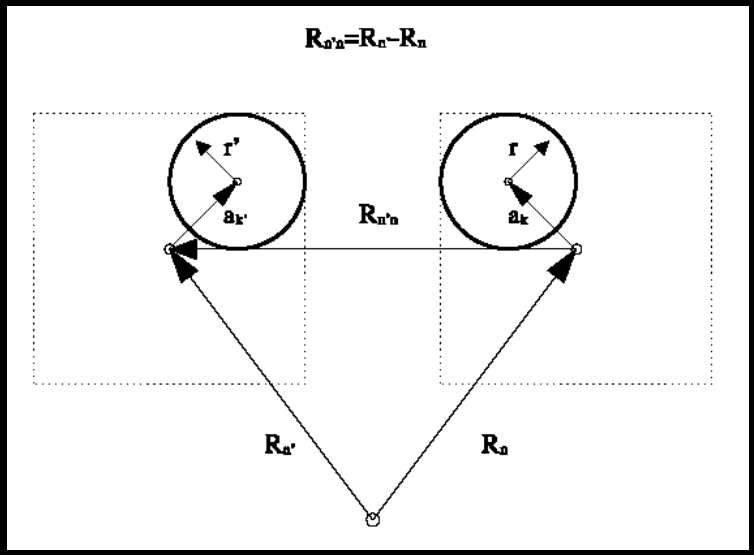

$$T = V + V G_0 T,$$

Path-scattering operator (for many potentials)

$$T = \sum_{i,k} [v_i \delta_{ik} + v_i \frac{1}{E - H_0 - v_i} \sum_{m \neq i} (v_i \delta_{mk} + v_m \frac{1}{E - H_0 - V} v_k)].$$

$$t = V + V g_0 t$$

$$G = g_0(1 + t g_0) + (1 + g_0 t)(g_r^{-1} - t)^{-1}(t g_0 + 1)$$

Scattering operator **τ** for single potential ***v***

$$T = \sum_{i,k} T^{i,k},$$

$$T^{i,k} = t_i \delta_{ik} + t_i G_0 \sum_{m \neq i} T^{m,k},$$

$$t_i = v_i + v_i G_0 t_i.$$

Multiple Scattering Theory (2)

$$G = G_0 + G_0 V G.$$

Korringa-Kohn-Rostoker method

$$G = g_0(1 + t g_0) + (1 + g_0 t)(g_r^{-1} - t)^{-1}(t g_0 + 1)$$

Expression of full GF

$$< \mathbf{r}' + \mathbf{a}_{k'} + \mathbf{R}_{n'} | G_0(E) | \mathbf{r} + \mathbf{a}_k + \mathbf{R}_n > =$$
$$-\frac{1}{4\pi} \frac{\exp\left[i\sqrt{E}|\mathbf{r}' + \mathbf{a}_{k'} + \mathbf{R}_{n'} - (\mathbf{r} + \mathbf{a}_k + \mathbf{R}_n)|\right]}{|\mathbf{r}' + \mathbf{a}_{k'} + \mathbf{R}_{n'} - (\mathbf{r} + \mathbf{a}_k + \mathbf{R}_n)|},$$

$$G_0 = g_0 + g_r,$$

$$t = V + V g_0 t$$

In spherical muffin-tin model matrices are site-diagonal

$$< \mathbf{r}' + \mathbf{a}_{k'} + \mathbf{R}_{n'} | g_0(E) | \mathbf{r} + \mathbf{a}_k + \mathbf{R}_n > =$$
$$\sum_{L'L} Y_{L'}(\hat{r}')[-i\sqrt{E} h_l^+(\sqrt{E} r_>) j_l(\sqrt{E} r_<)] Y_L(\hat{r}) \delta_{k'k} \delta_{n'n} \delta_{L'L},$$

Free-electron part

$$< \mathbf{r}' + \mathbf{a}_{k'} + \mathbf{R}_{n'} | g_r(E) | \mathbf{r} + \mathbf{a}_k + \mathbf{R}_n > =$$
$$\sum_{L'L} Y_{L'}(\hat{r}') j_{l'}(\sqrt{E} r') B^{(n'n)}_{k'L',kL} Y_L(\hat{r}) j_l(\sqrt{E} r).$$

Regular part

$$[B(\mathbf{k}, E)]_{k'L',kL} = \sum_{\mathbf{R}_{n'n}} \exp(i\mathbf{k}\mathbf{R}_{n'n}) [B(E)]^{(n'n)}_{k'L',kL}$$

KKR-constants matrix

Multiple Scattering Theory (3)

Korringa-Kohn-Rostoker method

$$Z_{\sigma L}^{(k)}(r) = j_l(\sqrt{E}r)\tau_{\sigma L}(E)^{-1} - i\sqrt{E}h_l(\sqrt{E}r).$$
$$J_{\sigma L}^{(k)}(r) = j_l(\sqrt{E}r),$$

Z(r) and *J(r)* - regular and irregular solutions of Schrodinger equation

$$< s'\mathbf{r}' + \mathbf{a}_{k'} + \mathbf{R}_{n'}|G(E)|s\mathbf{r} + \mathbf{a}_k + \mathbf{R} >= -\sum_{\sigma L} J_{\sigma L}^{(k)}(s'\mathbf{r}')Z_{\sigma L}^{(k)}(s\mathbf{r})\delta_{k'k}\delta_{n',n}$$
$$+ \sum_{\sigma' L',\sigma L} Z_{\sigma' L'}^{(k')}(s'\mathbf{r}')[\tau^{-1} - \mathbf{B}(E)]^{-1(n'n)}_{k'\sigma' L',k\sigma L} Z_{\sigma L}^{(k)}(s\mathbf{r}). \qquad (18)$$

$$< s'\mathbf{r}' + \mathbf{a}_{k'}|G(\mathbf{k}E)|s\mathbf{r} + \mathbf{a}_k >=$$
$$\sum_{\mathbf{R}_{n'n}} \exp(i\mathbf{k}\mathbf{R}_{n'n}) < s'\mathbf{r}' + \mathbf{a}_{k'} + \mathbf{R}_{n'}|G(E)|s\mathbf{r} + \mathbf{a}_k + \mathbf{R}_n >$$

$$< s'\mathbf{r}' + \mathbf{a}_{k'}|G(\mathbf{k}E)|s\mathbf{r} + \mathbf{a}_k >= -\sum_{\sigma L} J_{\sigma L}^{(k)}(s'\mathbf{r}')Z_{\sigma L}^{(k)}(s\mathbf{r})\delta_{k'k}$$
$$+ \sum_{\sigma' L',\sigma L} Z_{\sigma' L'}^{(k')}(s'\mathbf{r}')[\tau^{-1} - \mathbf{B}(\mathbf{k}E)]^{-1}_{k'\sigma' L',k\sigma L} Z_{\sigma L}^{(k)}(s\mathbf{r}).$$

$$\det|\tau^{-1} - \mathbf{B}(k, E)| = 0.$$

Novel formulation of KKR equations

Problem with eigenvalues functions

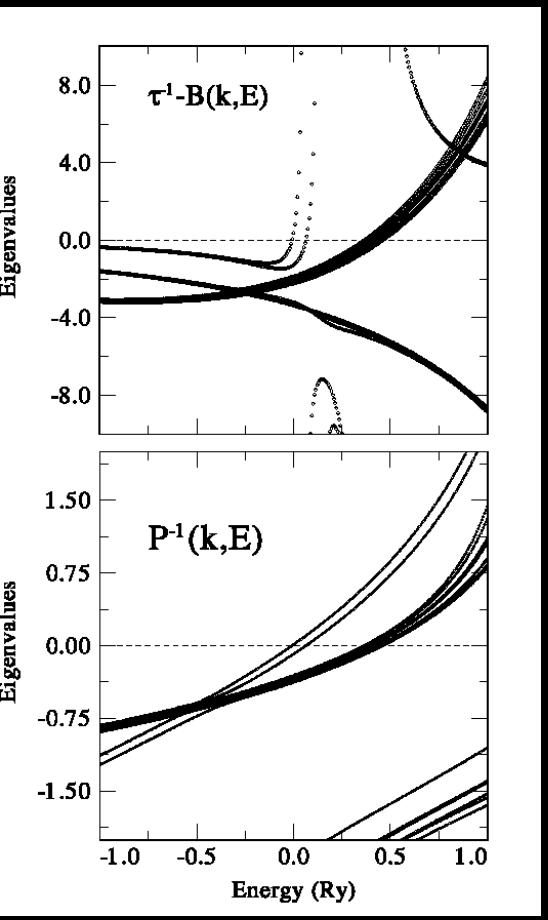

$$\zeta_l^{(k)}(r) = -J_l^{(k)}(r) Z_l^{(k)}(S_k) + Z_l^{(k)}(r) j_l(\sqrt{E} S_k).$$

$$\phi_l^{(k)}(r) = 1, \quad \zeta^{(k)}(S_k) = 0.$$

$$\phi_l^{(k)}(r) = Z_l^{(k)}(r) / Z_l^{(k)}(S_k),$$

$$< s' \mathbf{r}' + \mathbf{a}_{k'} | G(\mathbf{k}E) | s\mathbf{r} + \mathbf{a}_k > =$$
$$\sum_{\sigma' L' \sigma L} Y_{L'}(\hat{\mathbf{r}}') \chi_{\sigma'}(s') \{ \zeta_{\sigma' l'}(r') \phi_{\sigma l}(r) \delta_{\sigma' \sigma} \delta_{k' k} \delta_{L' L}$$
$$+ \phi_{\sigma' l'}(r') [\mathbf{g}_0(\mathbf{k}E, S)^{-1} - (\mathbf{D} - \mathbf{D}^{(j)})]^{-1}_{k' \sigma' L', k \sigma L} \phi_{\sigma l}(r) \} \chi_\sigma(s) Y_L(\hat{\mathbf{r}}).$$

$$D_{\sigma k l}(E) = S_k^2 \frac{\partial}{\partial r} \ln(\phi_{\sigma l}^{(k)}(r)|_{r=S_k}$$

$$D_{kl}^{(j)}(E) = S_k^2 \frac{\partial}{\partial r} \ln(j_l(r)|_{r=S_k}$$

- monotonic behaviour
- easy to extract E(k)
- important for computations with large number of atoms

$$\det |g_0^{-1}(\mathbf{k}, E, S) - (D - D_{(j)})| = 0$$

KKR-CPA method

Korringa-Kohn-Rostoker with coherent potential approximation

$$G(E)=\sum_{s=(+,-)}\sum_{k=1}^{K}\int_{V_k} d^3r\langle s,\mathbf{r}+\mathbf{a}_k|G(E)|s,\mathbf{r}+\mathbf{a}_k\rangle$$

ansil, Kaprzyk, Mijnarends, Tobola,
hys. Rev. B (1999) conventional KKR

Green function

Stopa, Kaprzyk, Tobola,
J.Phys.CM (2004)
novel formulation of KKR

$$\langle s',\mathbf{r}'+\mathbf{a}_{k_{CP}}|G^{A(B)}(E)|s,\mathbf{r}+\mathbf{a}_{k_{CP}}\rangle$$
$$=-\sum_{\sigma L} J^{A(B)}_{\sigma L}(s'\mathbf{r}')Z^{A(B)}_{\sigma L}(s\mathbf{r})$$
$$+\sum_{\sigma' L',\sigma L} Z^{A(B)}_{\sigma' L'}(s'\mathbf{r}')T^{A(B)}_{k_{CP}\sigma' L',k_{CP}\sigma L}Z^{A(B)}_{\sigma L}(s\mathbf{r})$$

$$\langle s',\mathbf{r}'+\mathbf{a}_{k'}|G(E)|s,\mathbf{r}+\mathbf{a}_k\rangle$$
$$=-\sum_{\sigma L} J^{(k)}_{\sigma L}(s'\mathbf{r}')Z^{(k)}_{\sigma L}(s\mathbf{r})\delta_{kk'}$$
$$+\sum_{\sigma' L',\sigma L} Z^{(k')}_{\sigma' L'}(s'\mathbf{r}')T^{CP}_{k'\sigma' L',k\sigma L}Z^{(k)}_{\sigma L}(s\mathbf{r})$$

$$(E)=-\frac{d}{dE}\left\{\frac{1}{N}\sum_{\mathbf{k}\in BZ}\mathrm{Tr}\ln[G_0^{-1}(E,\mathbf{k})+D^{(j)}-D_{CP}]^{-1}\right\}$$
$$-\frac{d}{dE}\{c_A\mathrm{Tr}\ln[\Psi_A^{-1}G^A]+c_B\mathrm{Tr}\ln[\Psi_B^{-1}G^B]$$
$$-\mathrm{Tr}\ln G^{CP}\}+\frac{d}{dE}\left\{\sum_{k\neq k_{CP}}\mathrm{Tr}\ln[\Psi^{(k)}]\right\},\qquad(2.22)$$

$$T^{CP}_{k'\sigma' L',k\sigma L}=\frac{1}{N}\sum_{\mathbf{k}\in BZ}[\tau_{CP}^{-1}-B(E,\mathbf{k})]^{-1}_{k'\sigma' L',k\sigma L}$$

CPA $\quad c_A T^A+c_B T^B=T^{CP}$

Density of states $\quad N(E)=-\frac{1}{\pi}\mathrm{Im}\int_{-\infty}^{E}dE\,G(E)$

loyd formula Kaprzyk et al. Phys. Rev. B (1990) Fermi energy $N(E_F)=Z$

Ground state properies

KKR-CPA code (S. Kaprzyk)

Total density of states DOS

$$N(E) = -\frac{1}{\pi}\,\mathrm{Im}\int_{-\infty}^{E} dE\,G(E)$$

Component, partial DOS

$$\rho_\sigma(E) = \frac{\partial}{\partial E} N_\sigma(E)$$

Total magnetic moment

$$\mu = N_+(E_F) - N_-(E_F)$$

Spin and charge densities

$$\rho_\sigma^{(k)}(\mathbf{r}) = -\frac{1}{\pi}\int_{-\infty}^{E_F} dE \langle \sigma, \mathbf{r}+\mathbf{a}_k | G(E) | \sigma, \mathbf{r}+\mathbf{a}_k \rangle$$

Local magnetic moments

$$\mu^{(k)} = \mu_B \int_{\Omega_k} d^3 r s^{(k)}(\mathbf{r})$$

Fermi contact hyperfine field

$$H_{Fermi} = \frac{8}{3}\pi\mu_B[\rho_\uparrow(0) - \rho_\downarrow(0)]$$

Bands E(**k**), total energy, electron-phonon coupling (superconductivity), magnetic structures, transport properties, magnetocaloric, photoemission spectra, Compton profiles

Metal-semiconductor-metal crossovers

Toboła, et al., PRB (2001)

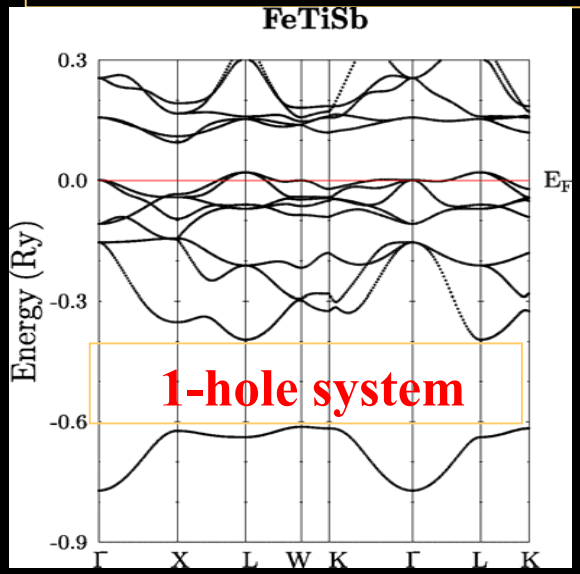

FeTiSb (VEC=17)

Curie-Weiss PM

($0.87\mu_B$)

NiTiSb (VEC=19)

Pauli PM

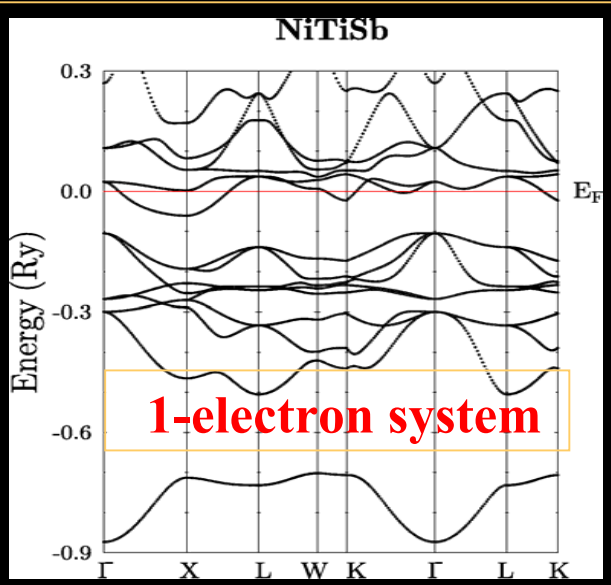

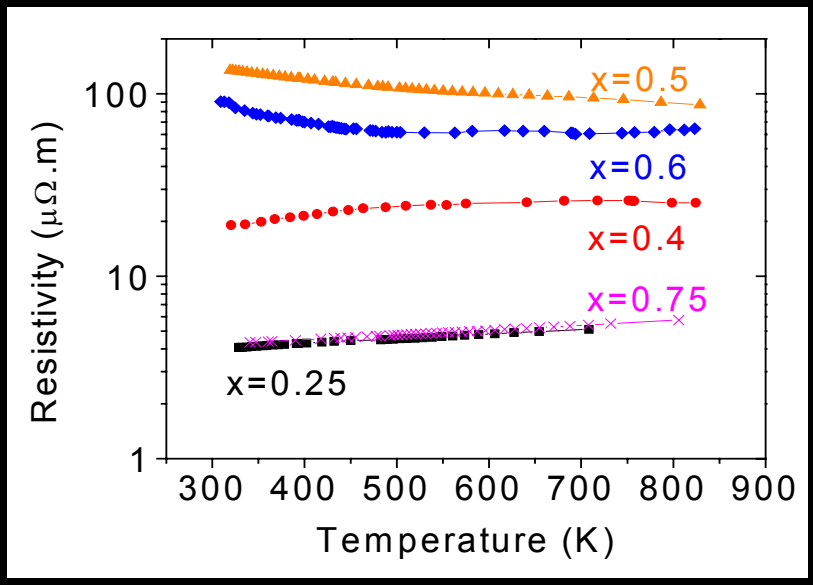

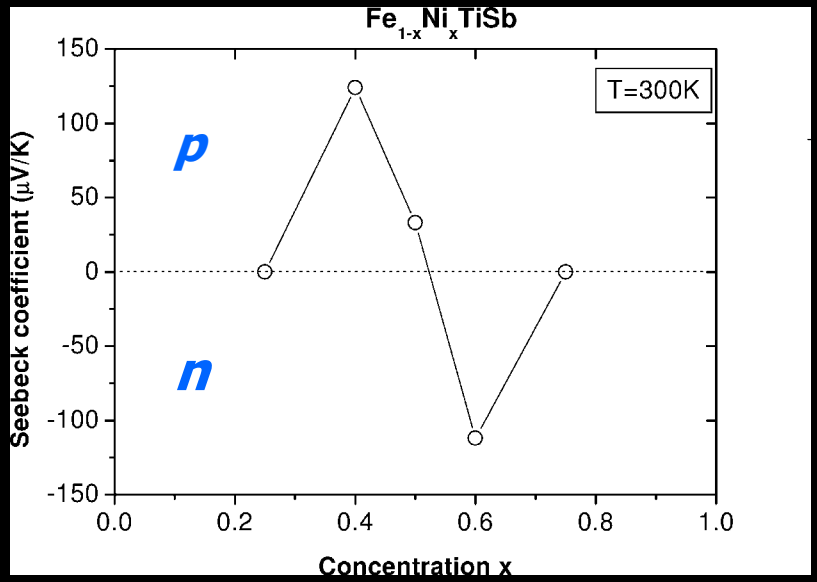

Resistivity

Seebeck coefficient

Semiconductor from alloyed metals

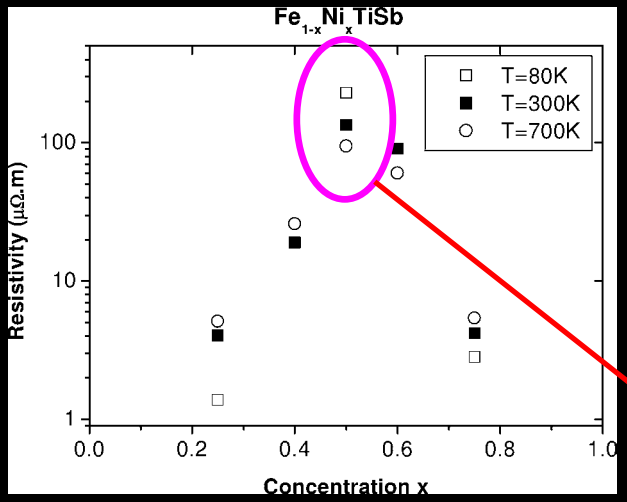

Resistivity

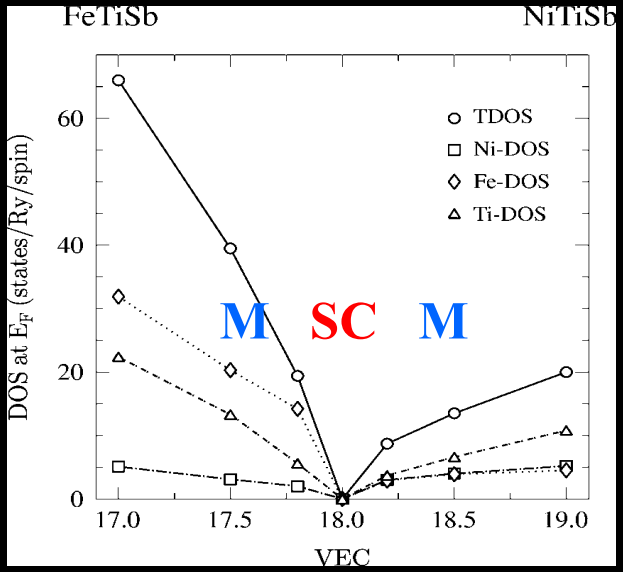

Density of states at E_F

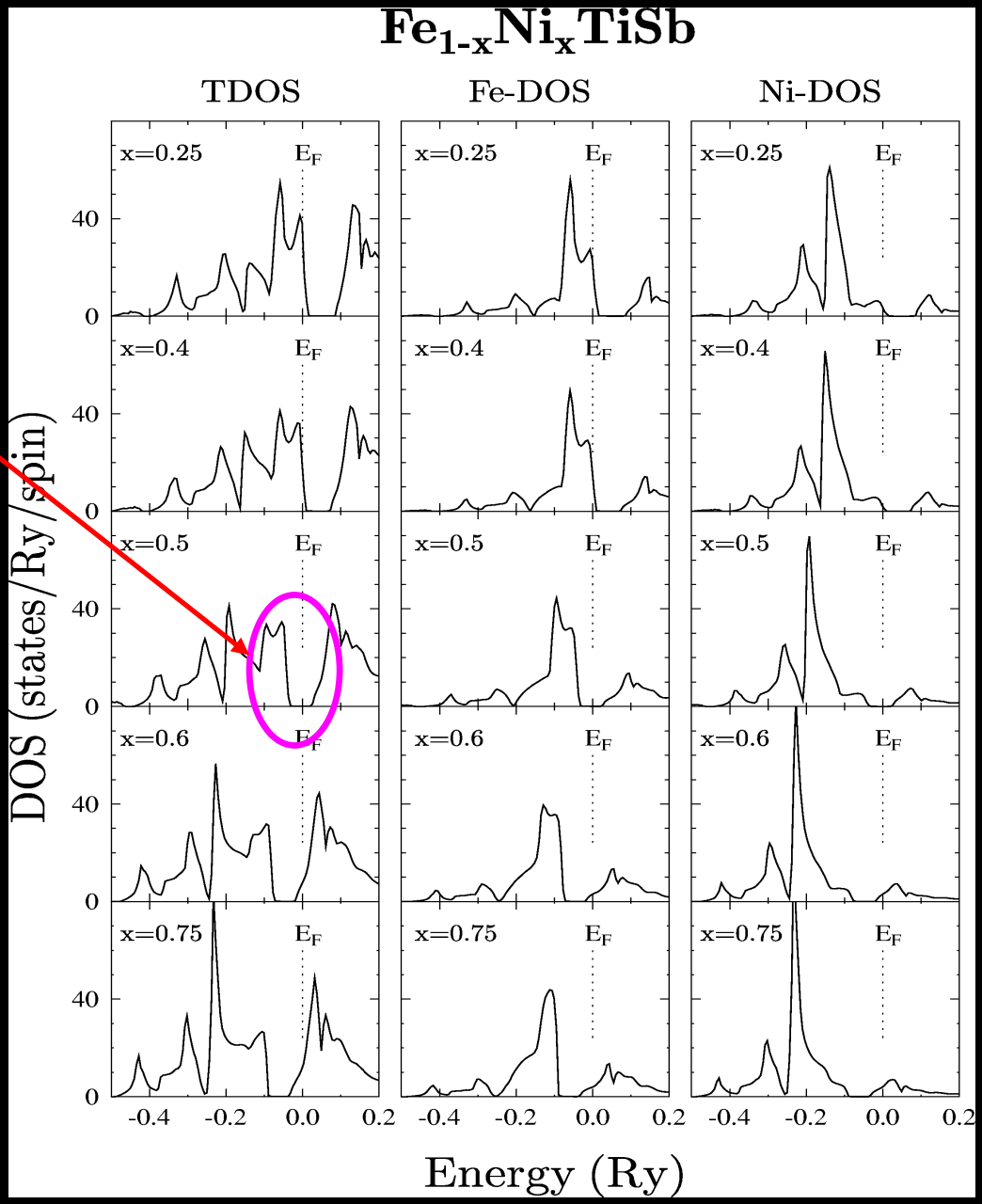

INS SC M

Thermoelectric properties

Resistivity

Seebeck coefficient

Thermal conductivity

Figure of merit ZT

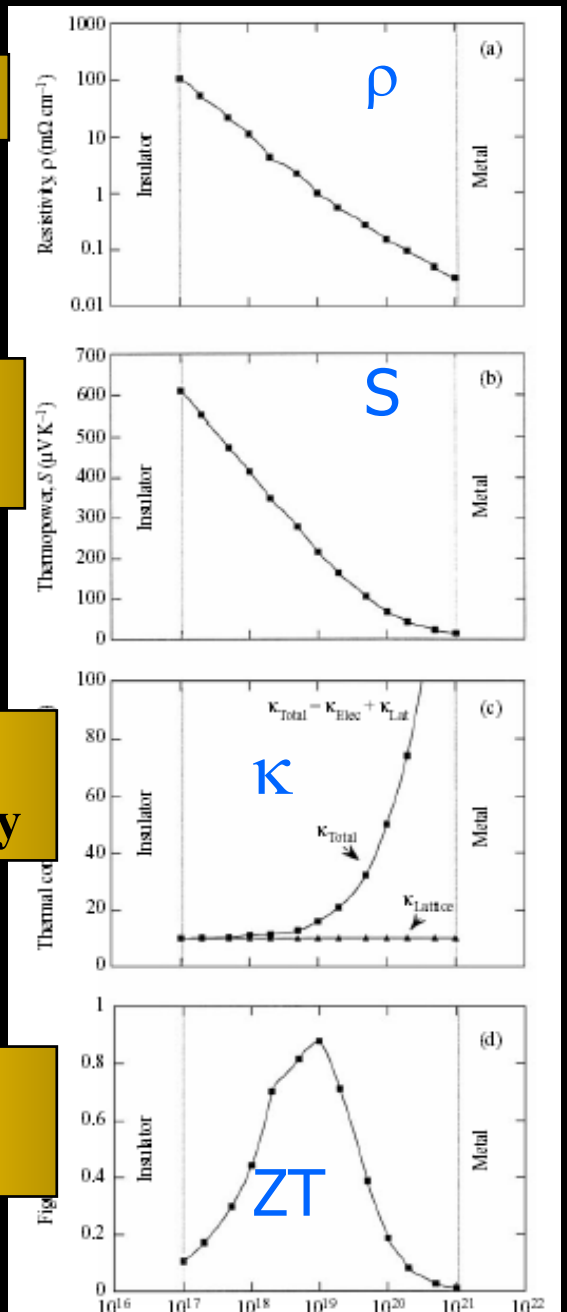

$$ZT = \frac{S^2}{\rho \kappa}$$

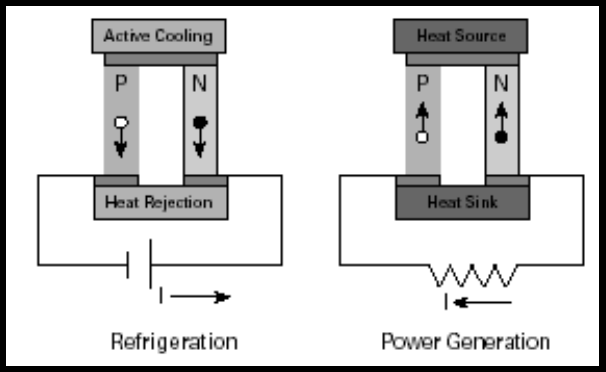

Example: FeVSb doped with Ti

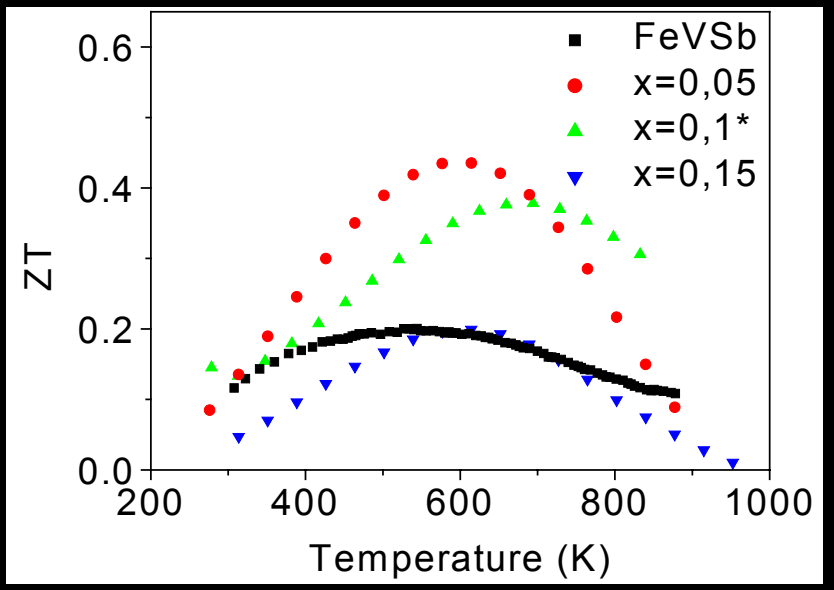

L. Jodin (PhD Thesis)

„Czworobok" termoelektryczny

$$\begin{bmatrix} \rho \\ j \\ \rho \\ q \end{bmatrix} = \begin{bmatrix} L_{EE} & L_{ET} \\ L_{TE} & L_{TT} \end{bmatrix} \begin{bmatrix} \rho \\ E \\ \rho \\ -\nabla T \end{bmatrix}$$

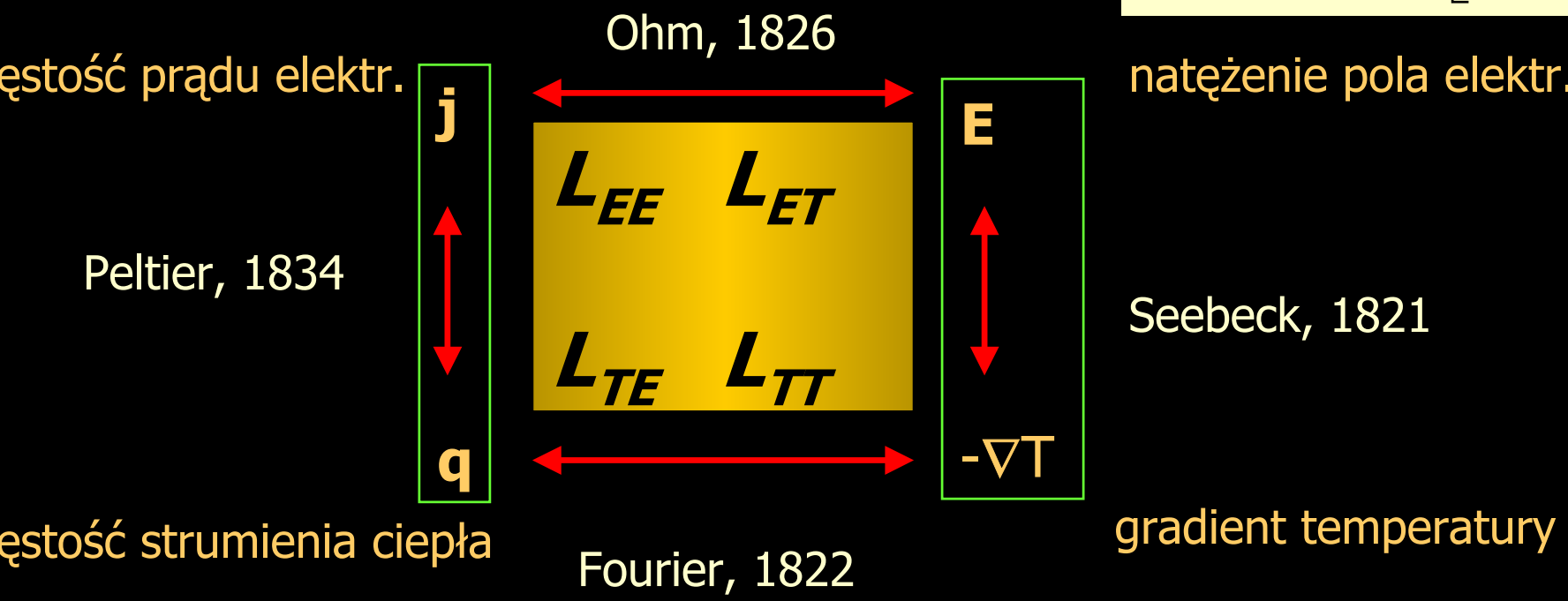

S= Π T (Kelvin-Onsager) $L_{ET}=L_{TE}/T$

$\kappa/\sigma \approx L_0 T$ (Wiedemann-Franz, L_0 liczba Lorentza) $\kappa \approx -L_{TT}$

$$\begin{bmatrix} \rho j \\ \rho q \end{bmatrix} = \begin{bmatrix} L_{EE} & L_{ET} \\ L_{TE} & L_{TT} \end{bmatrix} \begin{bmatrix} \rho E \\ \rho -\nabla T \end{bmatrix}$$

Efekt Seebecka (1821)

1770 Tallin
1854 Berlin

natężenie pola elektr. **E= S ∇ T** gradient temperatury

siła termoelektryczna $S = L_{EE}^{-1} L_{ET}$

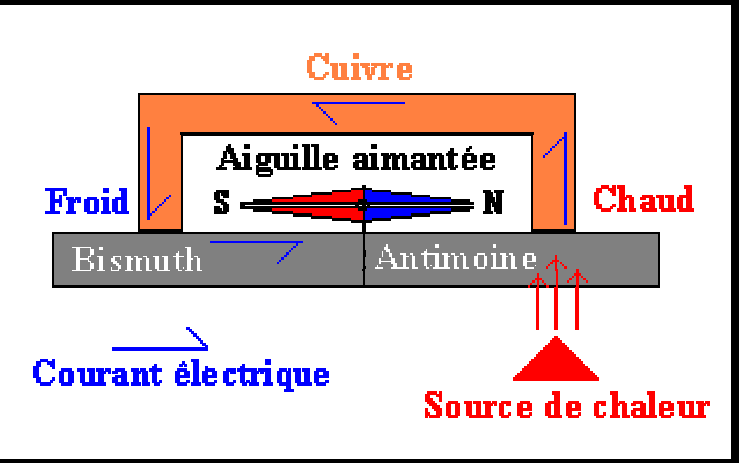

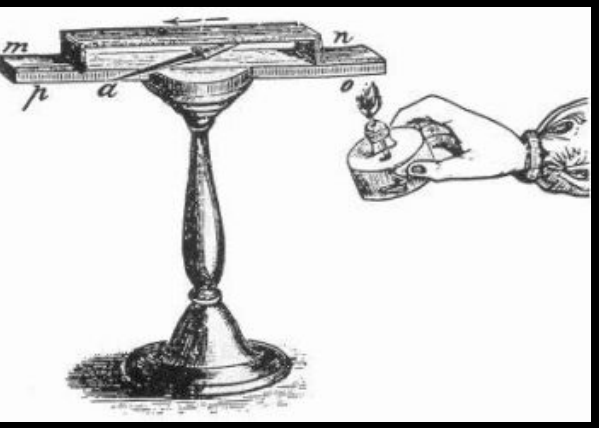

Barwna postać romantyzmu

- wraz z Goethe tworzy nową teorię barw (przeciwną Newtonowi),
- gradient temperatur powoduje zmiany pola magnetycznego Ziemi !!,
- doświadczenia Oersteda (1820) – „oślepiają" uczonych; odkrycie elektromagnetyzmu

Wyjaśnienie : termomagnetyzm - „magnetyczna" polaryzacja metali i stopów wskutek różnicy temperatur !!

$$\begin{bmatrix} \rho \\ j \\ \rho \\ q \end{bmatrix} = \begin{bmatrix} L_{EE} & L_{ET} \\ L_{TE} & L_{TT} \end{bmatrix} \begin{bmatrix} \rho \\ E \\ \rho \\ -\nabla T \end{bmatrix}$$

Relacja Fouriera (1822)

1768 Auxerre
1830 Paris

ęstość strumienia ciepła **q**= -κ ∇ T gradient temperatury

przewodność cieplna $\kappa = L_{TE}L_{EE}^{-1}L_{ET} - L_{TT}$

$$\kappa = \frac{3}{2}\frac{n}{m} k_B \tau T$$

Ciepło rzewodzone netto = Ciepło generowane wewnątrz - Ciepło zatrzymane wewnątrz

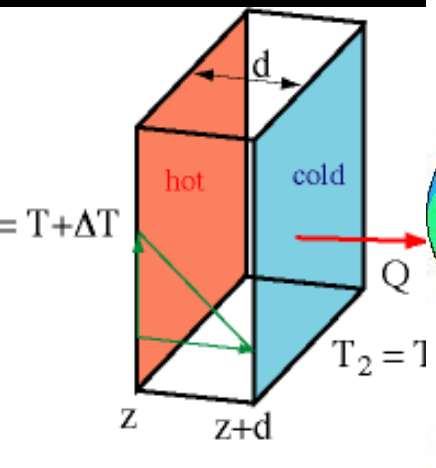

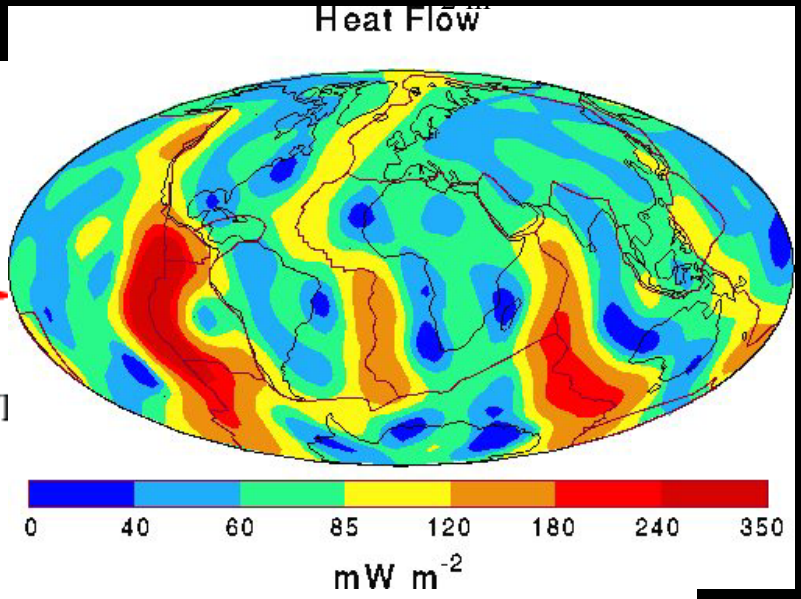

in differential form: $Q(z) = -k\frac{dT}{dz}$

$\nabla \mathbf{q} = q_{gen} - du/dt$

$du/dt = \rho\, c\, dT/dt$

$\nabla(-\kappa \nabla T) + \partial T/\partial t = q_{gen}$

$\nabla^2 T + (\rho c/k)\, \partial T/\partial t = 0$

gdy $q_{gen}=0$

$$\begin{bmatrix} \rho j \\ \rho q \end{bmatrix} = \begin{bmatrix} L_{EE} & L_{ET} \\ L_{TE} & L_{TT} \end{bmatrix} \begin{bmatrix} \rho E \\ \rho(-\nabla T) \end{bmatrix}$$

Prawo Ohma (1826)

1789 Erlangen
1854 Monachiu

gęstość prądu elektr. $\mathbf{j} = \sigma \mathbf{E}$ natężenie pola elektr.

przewodność elektryczna $\sigma = L_{EE} = ne\mu = ne\tau/m$

badania Ohma inspirowane pracami Fouriera i Seebecka

drut metalowy w cylindrze

- wychylenie igły magnetycznej propocjonalne do prądu I
- źródłem potencjału elektr. V – termopara Seebecka

$V/I = R$ (stałe gdy R stałe)

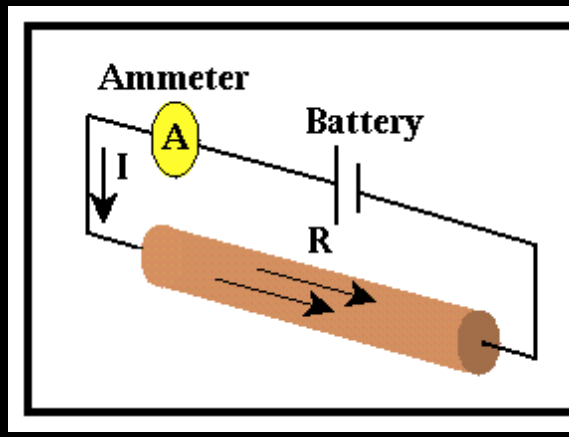

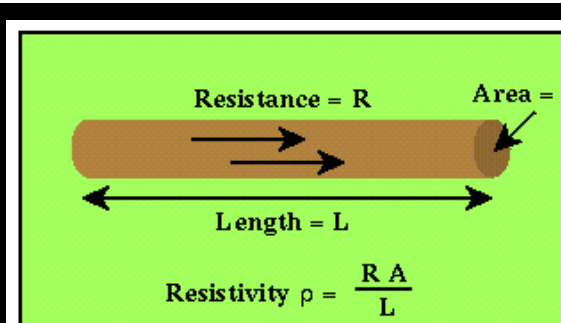

The Galvanic Circuit Investigated Mathematically" (1827)

$$\begin{bmatrix} \rho j \\ \rho q \end{bmatrix} = \begin{bmatrix} L_{EE} & L_{ET} \\ L_{TE} & L_{TT} \end{bmatrix} \begin{bmatrix} \rho E \\ \rho -\nabla T \end{bmatrix}$$

Efekt Peltier (1834)

zegarmistrz

strumień ciepła **q= Π j** gęstość prądu

współczynnik Peltier $\Pi = L_{TE} L_{EE}^{-1}$

1785 Ham
1845 Paris

odwrotny proces do efektu Seebecka

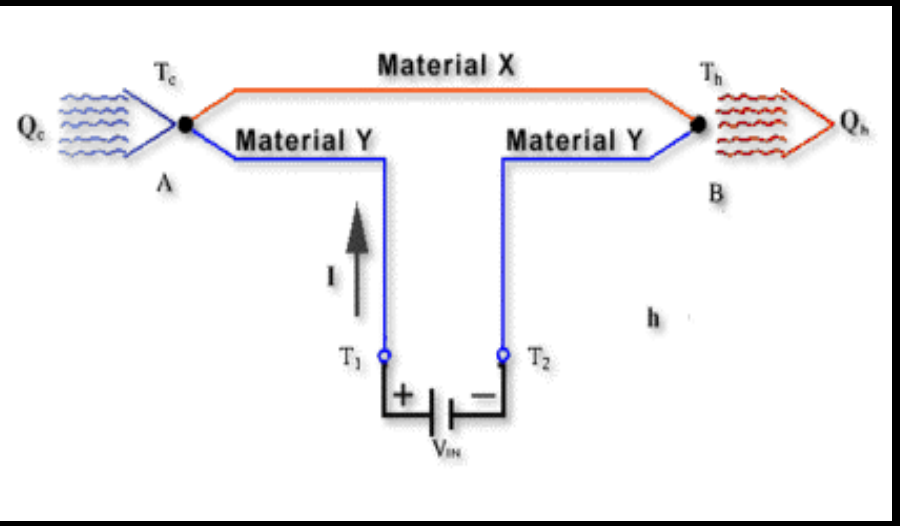

Efekt Thomsona (1834)

wydzielanie się ciepła w obecności prądu j i gradientu temperatury dT/dx

$$Q = j^2/\sigma + \mu\ j\ dT/dx$$

Joule Thomson

$$\mu = T\ dS/dT$$

$$\Pi = T\ S$$

$$\begin{bmatrix} J_Q \\ J \end{bmatrix} = \begin{bmatrix} L_{EE} & L_{ET} \\ L_{TE} & L_{TT} \end{bmatrix} \begin{bmatrix} \rho E \\ \rho \nabla T \end{bmatrix}$$

Ziman kinetic theory

$$\sigma(T) = e^2/3 \int dE\, N(E)\, v^2(E)\, \tau(E,T)\, [-\partial f(E)/\partial E]$$

Electrical conductivity

$$S(T) = e(3T\sigma)^{-1} \int dE\, N(E)\, v^2(E)\, E\, \tau(E,T)\, [-\partial f(E)/\partial E] =$$

$$(3eT\sigma)^{-1} \int dE\, \sigma(E,T)\, E\, [-\partial f(E)/\partial E]$$

Thermopower (Seebeck coefficient)

$$N(E) = (2\pi)^{-3} \int \delta(E(\mathbf{k})-E)\, d\mathbf{k}$$

DOS (density of states)

Thermal conductivity

$\kappa/\sigma \approx L_0 T$, $L_0 = 2.45$ $\kappa \approx -L_{TT}$

prawo Wiedemanna-Franza, L_0 liczba Lorentza

Boltzmann equation solutions

Calculations of residual conductivity and thermopower in alloys

$$\sigma(E) = \frac{2e^2}{3(2\pi)^3\hbar} \int_{\Sigma(E)} dS_{\mathbf{k}} v_{\mathbf{k}} \tau_{\mathbf{k}}$$

$$S = -\frac{\pi^2}{3}\frac{k_B^2 T}{e}\left.\frac{\partial \ln \sigma(E)}{\partial E}\right|_{E_F}$$

Conductivity

Thermopower

$$\mathbf{v_k} = \frac{1}{\hbar}\nabla_{\mathbf{k}}\left[ReE(\mathbf{k})\right]$$

Group velocity of electrons

$$\tau_{\mathbf{k}} = \frac{h}{ImE(\mathbf{k})}$$

Life-time of electrons (due to disorder)

x	$\rho_{calc}^{0K}(\mu\Omega m)$	$\rho_{exp}^{300K}(\mu\Omega m)$
0.25	0.15	4.1
0.4	0.64	19.1
0.5	∞	134.7
0.6	1.13	90.8
0.75	0.31	4.2

x	$S/T(\mu V/K^2)$	$S/T\cdot 300K(\mu V/K)$	$S_{exp}^{300K}(\mu V/K)$
0.25	-0.04	-12	≈ 0
0.4	0.4	120	124
0.5	0	0	33
0.6	-0.13	-39	-112
0.75	-0.05	-15	≈ 0

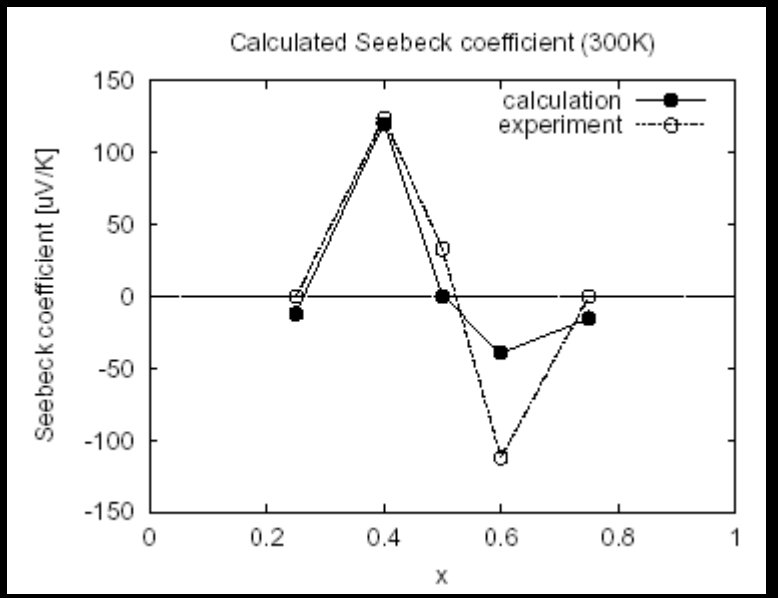

Stopa, Tobola, Kaprzyk, European Conference on Thermoelectrics 2004

Badanie stanów elektronowych w pobliżu powierzchni Fermiego $E(\mathbf{k})=E_F$

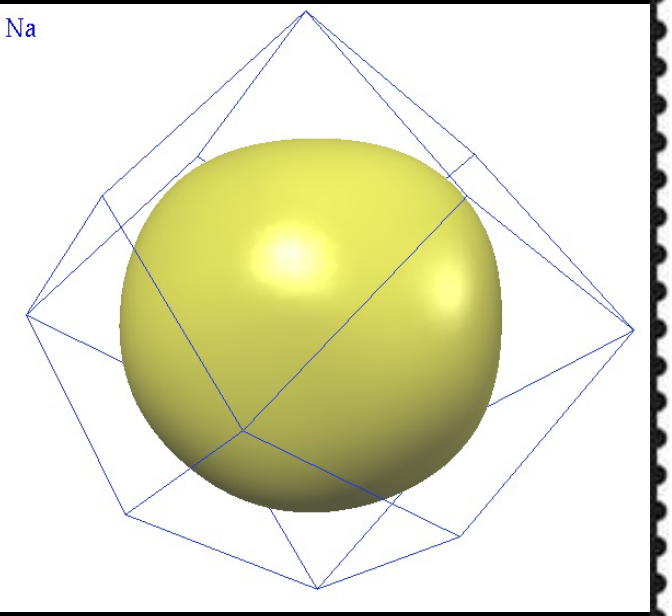

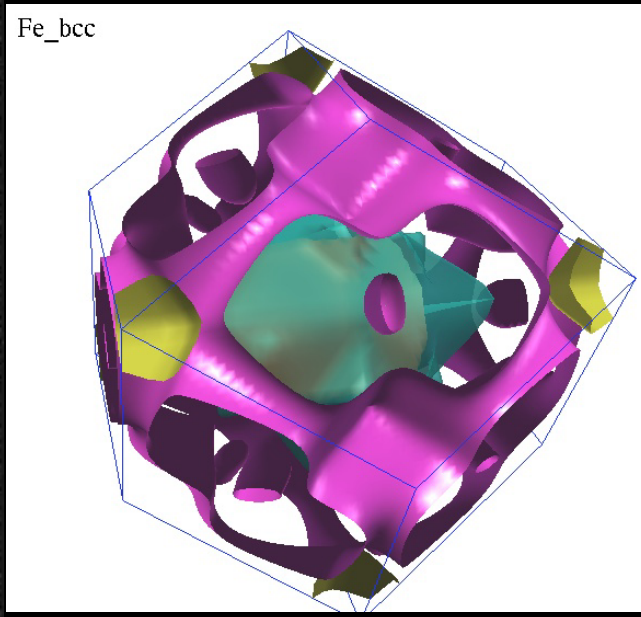

$$E(\vec{k}) = \frac{\eta^2(k_x^2 + k_y^2 + k_z^2)}{2m}$$

Calculations of residual conductivity and thermopower in alloys

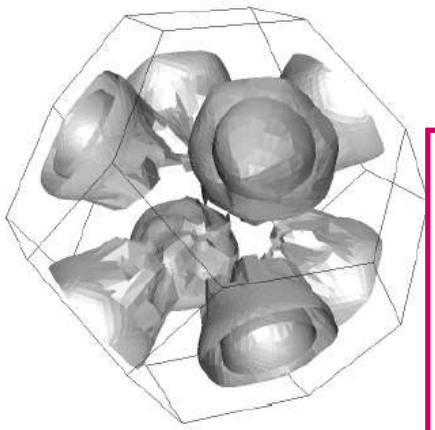

FIG. 7: Fermi surface of $Fe_{0.75}Ni_{0.25}TiSb$ ($x = 0.25$).

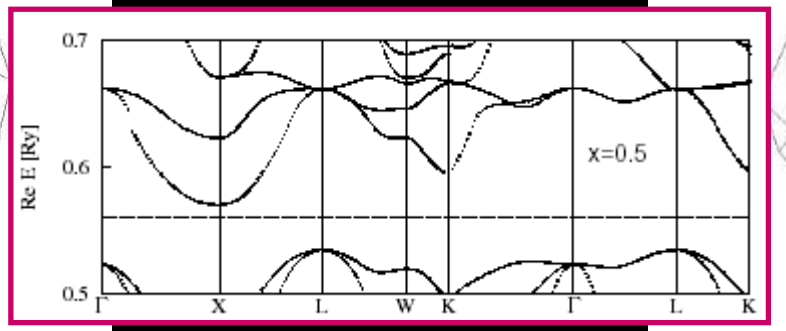

Semiconductor
x =0.50

Fermi surface peculiarities

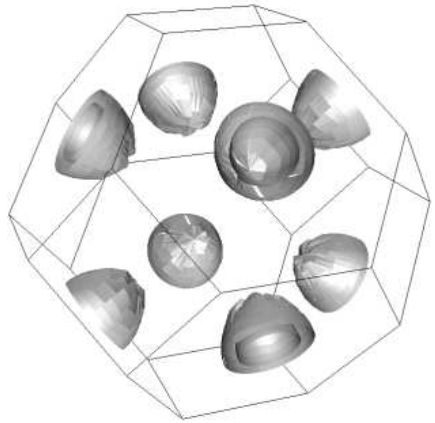

FIG. 8: Fermi surface of $Fe_{0.6}Ni_{0.4}TiSb$ ($x = 0.4$).

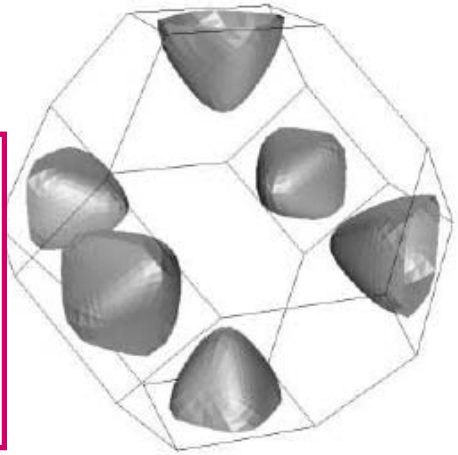

FIG. 9: Fermi surface of $Fe_{0.4}Ni_{0.6}TiSb$ ($x = 0.6$).

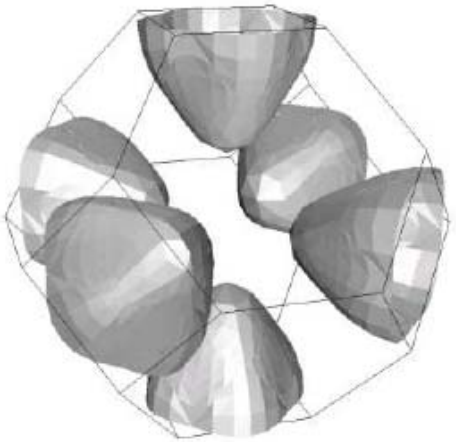

FIG. 10: Fermi surface of $Fe_{0.25}Ni_{0.75}TiSb$ ($x = 0.75$).

Search for new disordered SC

Total energy KKR analysis in Rh-Zr-Sb

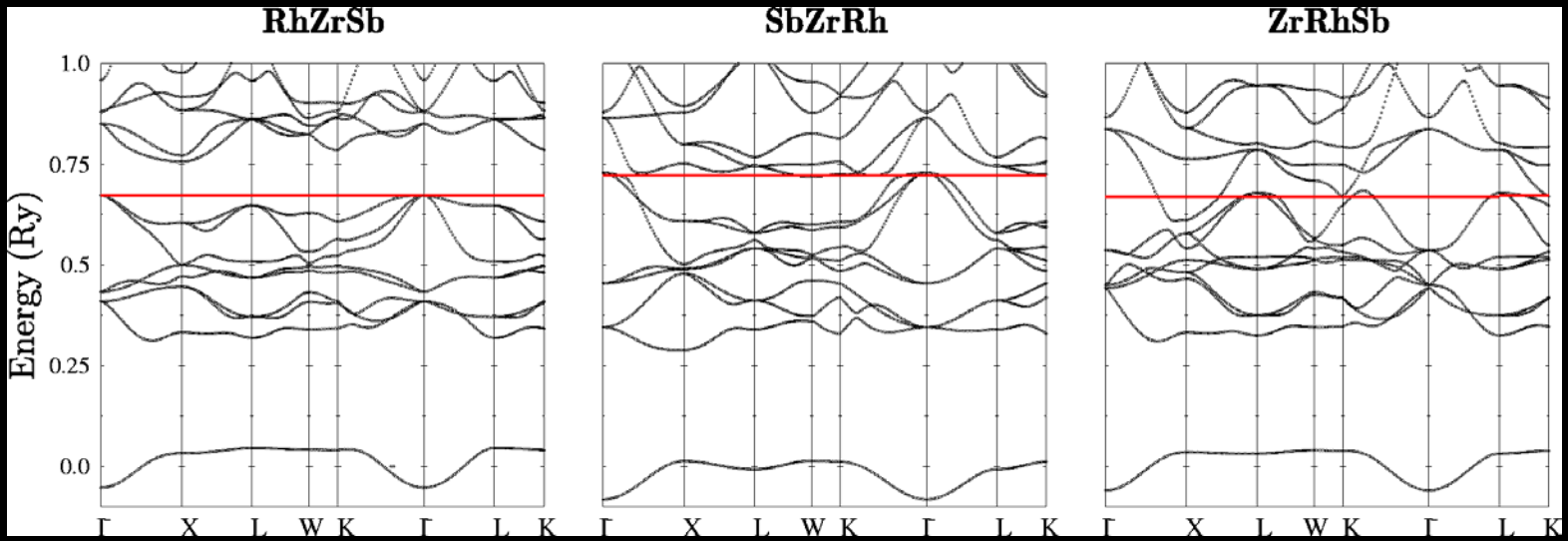

semiconductor semimetal metal

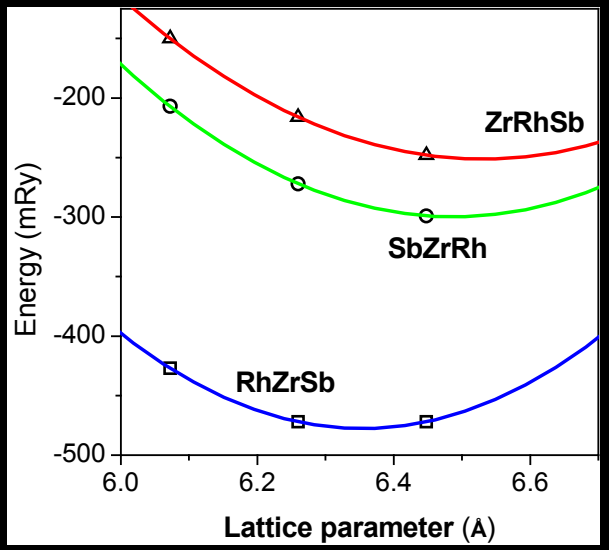

3 configurations

XYZ (=XZY)
YXZ (=YZX)
ZXY (=ZYX)

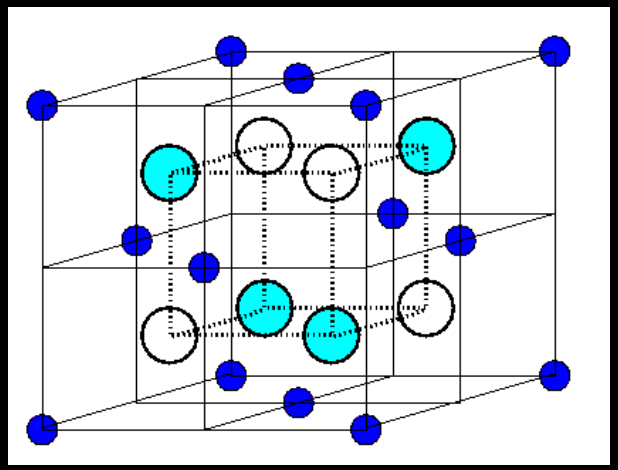

Larson et al., PRB (2002) - FLAPW

SC phase - the most STABLE

KKR-CPA density of states

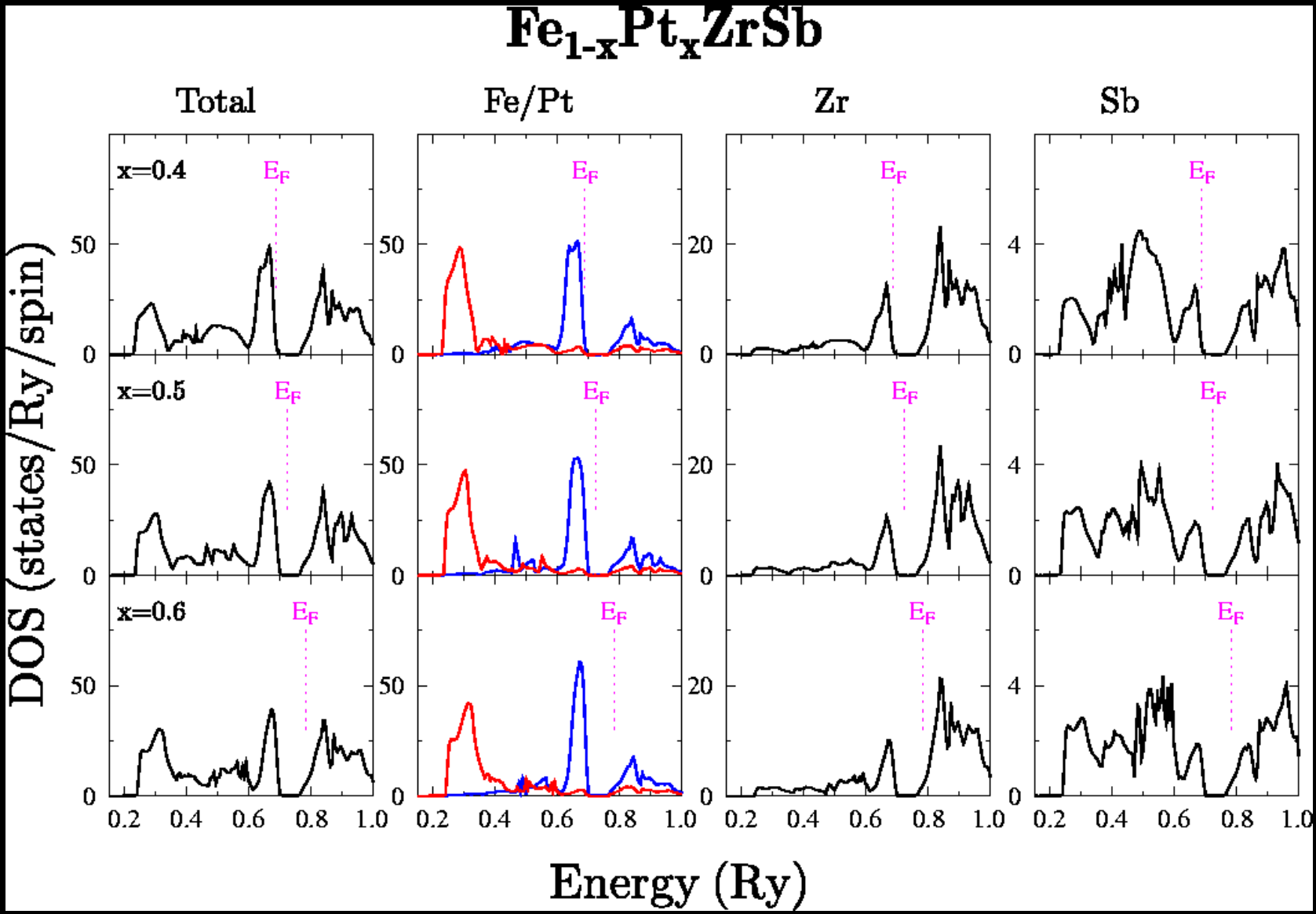

New half-Heusler phases close to VEC=18

Compound	a (Å)
$Fe_{1-x}Pt_xZrSb$	
x=0.4	**6.221(4)**
x=0.5	**6.231(5)**
x=0.6	**6.242(2)**
$Fe_{1-x}Ni_xHfSb$	
x=0.4	**6.063(5)**
x=0.5	**6.060(4)**
x=0.6	**6.048(6)**
$Fe_{1-x}Ni_xTiSb$	
x=0.4	**5.917(4)**
x=0.5	**5.910(3)**
x=0.6	**5.906(4)**
RhZrSb	**6.260(5)**
CoTiSb	**5.884(2)**

- **corresponding mixtures were first molten in an induction furnace in a water cooled copper crucible;**
- **resulting ingots were sealed in silica tube under argon and annealed during one week at 1073K;**
- **purity of the sample was checked by powder X-ray diffraction (Guinier camera Co K_α);**
- **cell parameters have been refined by a least square procedure from powder X-ray diffraction data recorded with high purity silicon (a = 5.43082 Å) as internal standard.**

Resistivity measurements

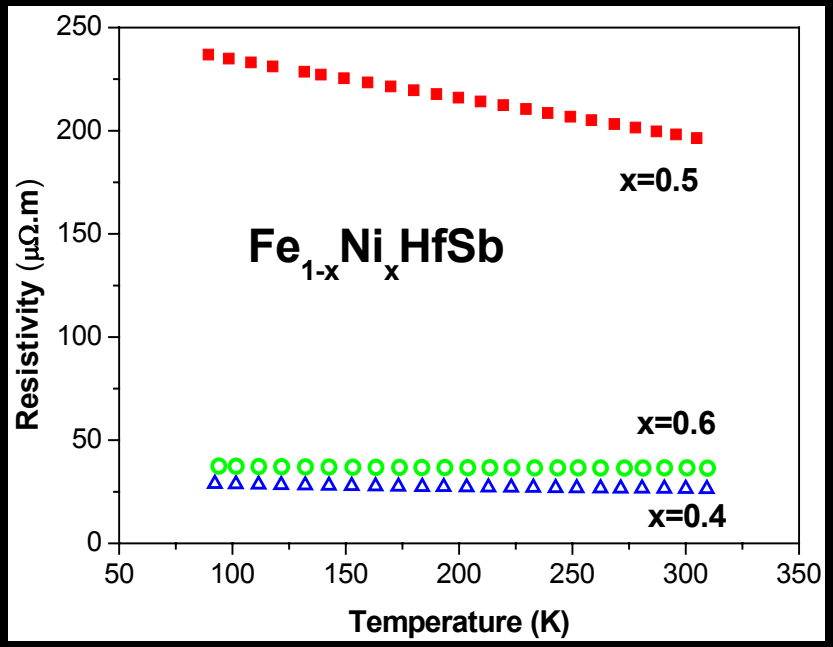

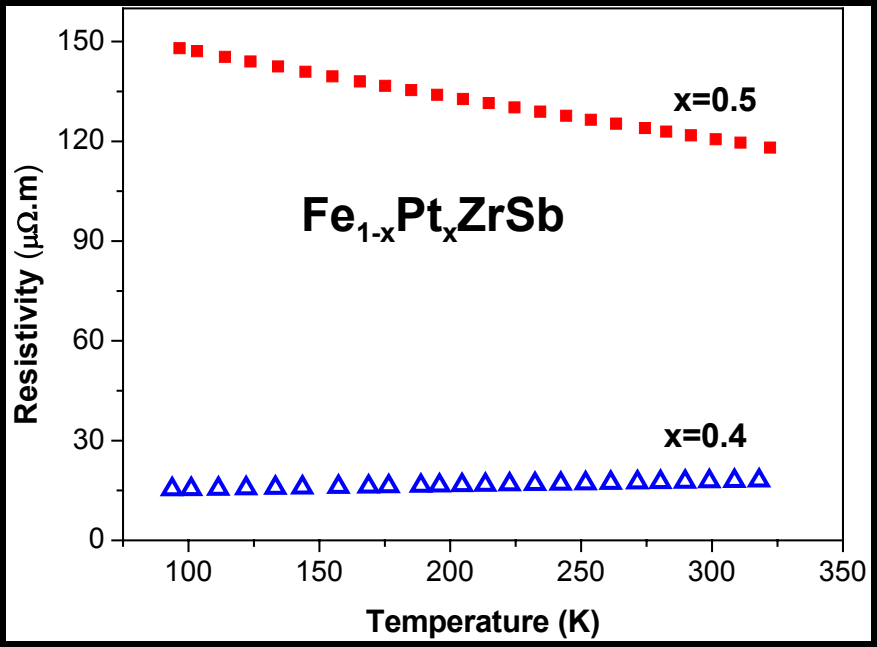

1) Resistivity decreases with T for x=0.5 in both series of compounds in semiconducting-like way ($d\rho/dT < 0$)

2) In other samples resistivity is also high but remains almost constant with T - conductivity limited by disorder scattering ($d\rho/dT \sim 0$)

3) Absolute values decrease comparing x=0.5 and other concentrations
   5-6 times $Fe_{1-x}Ni_xHfSb$
   8-10 times $Fe_{1-x}Pt_xZrSb$

Thermopower measurements

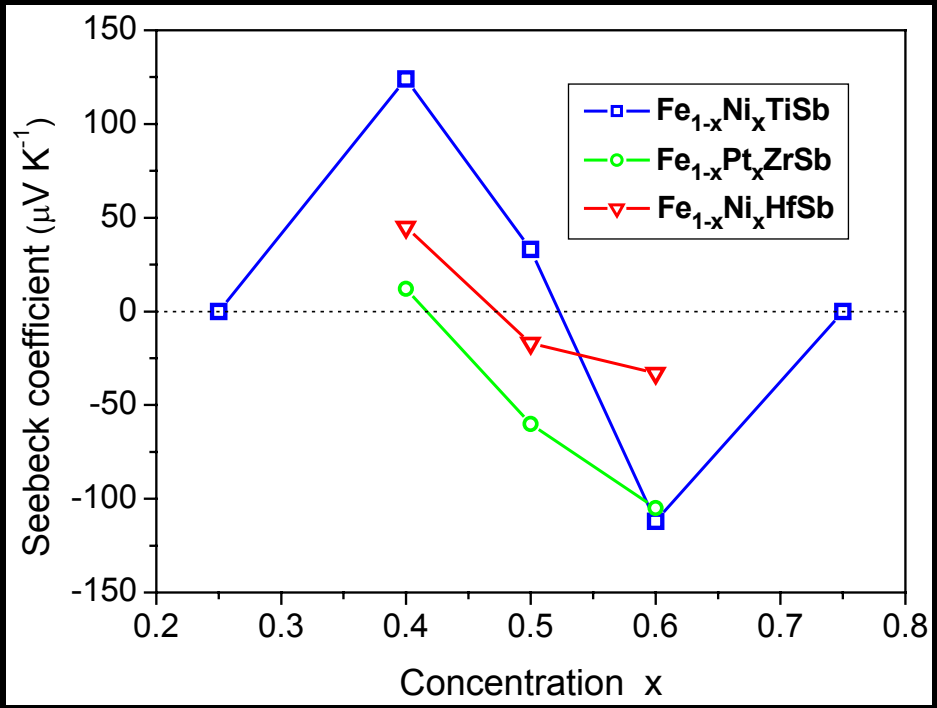

1) Seebeck coefficient changes in sign when approaching x=0.5.

2) Differences in critical concentration may arrise from crystal defects. Large values of S can be tentatively related to the DOS variations near the valence/conduction band edge (dn(E)/dE)

3) The thermoelectrical properties can be easily tuned by varying the sample composition.

Electronic structure peculiarities

ffect of Fermi shape on transport roperties in (Fe-Ni)TiSb
y T. Stopa

Half-Heusler (VEC=18)
Semiconductors/semimetals
(CoTiSb, NiTiSn, FeVSb, ...)
9 + 4 + 5=18

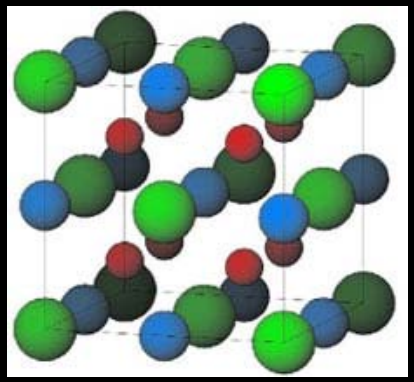

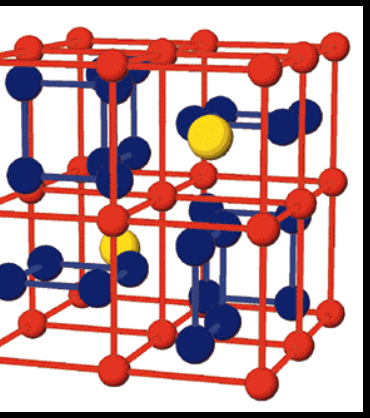

Skutterudites (VEC=96)
semiconductors/semimetals
($CoSb_3$, $RhSb_3$, $IrSb_3$, CoP_3 ...)
4 x 9 +12 x 5 = 96

Study of transport properties and electronic structure of $(Co\text{-}Rh)Sb_3$
by K. Wojciechowski

Chevrel phases (VEC=72)
semiconductors/semimetals
($TiMo_6Se_8$, $Zn_2Mo_6Se_8$, ...)
8 x 4 + 6 x 6 = 68 (*p-d* Mo_6Se_8)
4 holes to energy gap

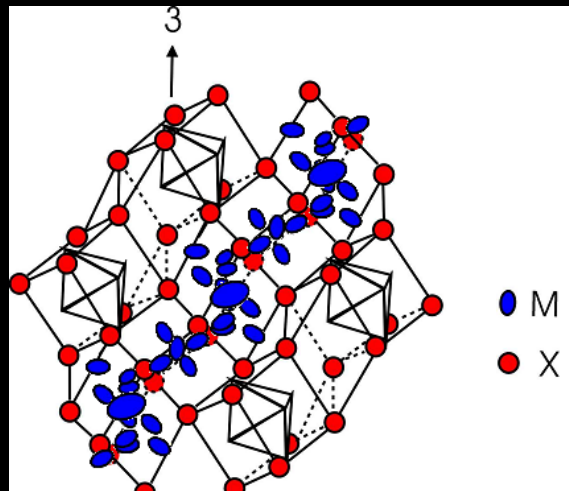

Chevrel phases

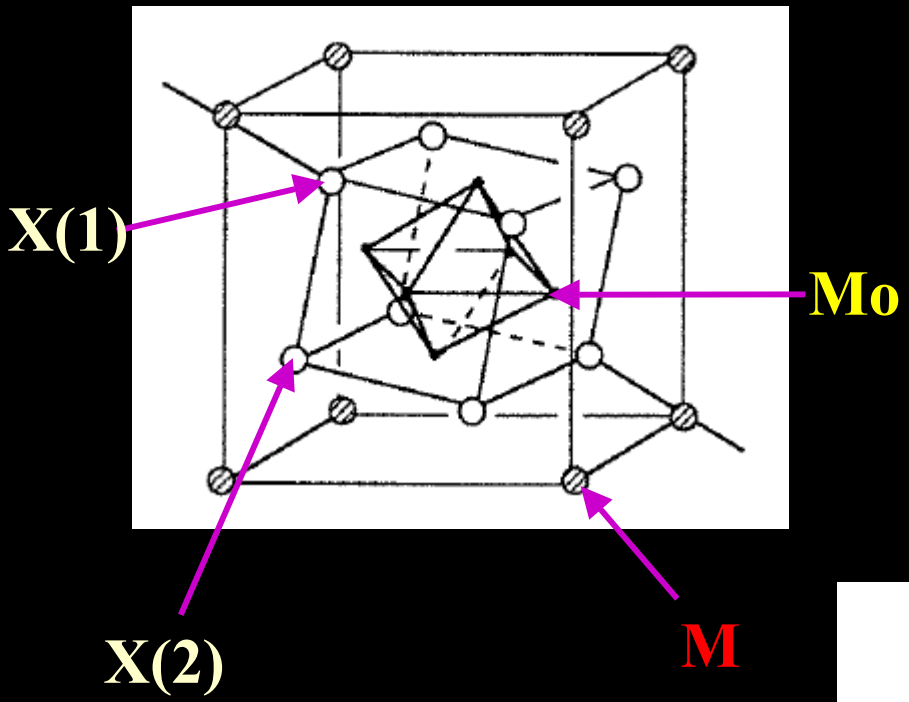

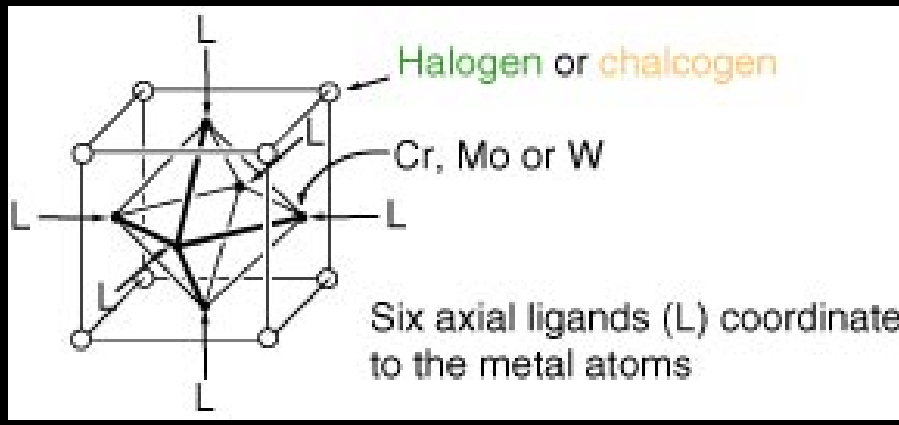

R-3 (rhomboedral)

Mo (6f) : (x,y,z)

Se (6f) : (x,y,z)

Se (2e) : (x,x,x)

M (1a) : (0,0,0) big cations (Sn, Pb)

M (6f) : (x,y,z) small cations (Cu, Zn)

P-3 triclinic

both open structures

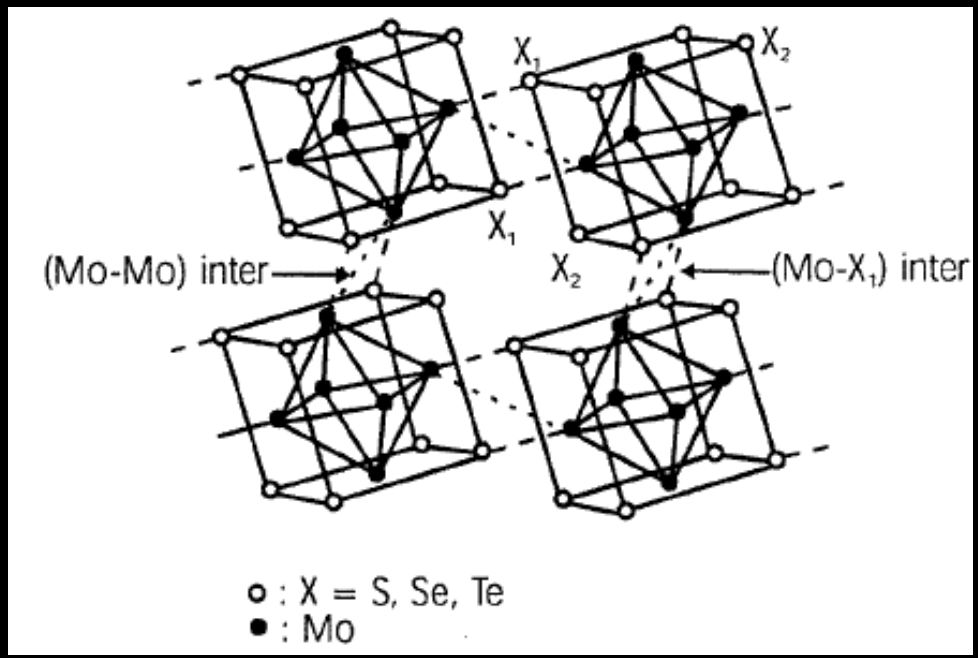

Chevrel phases with defects (2)

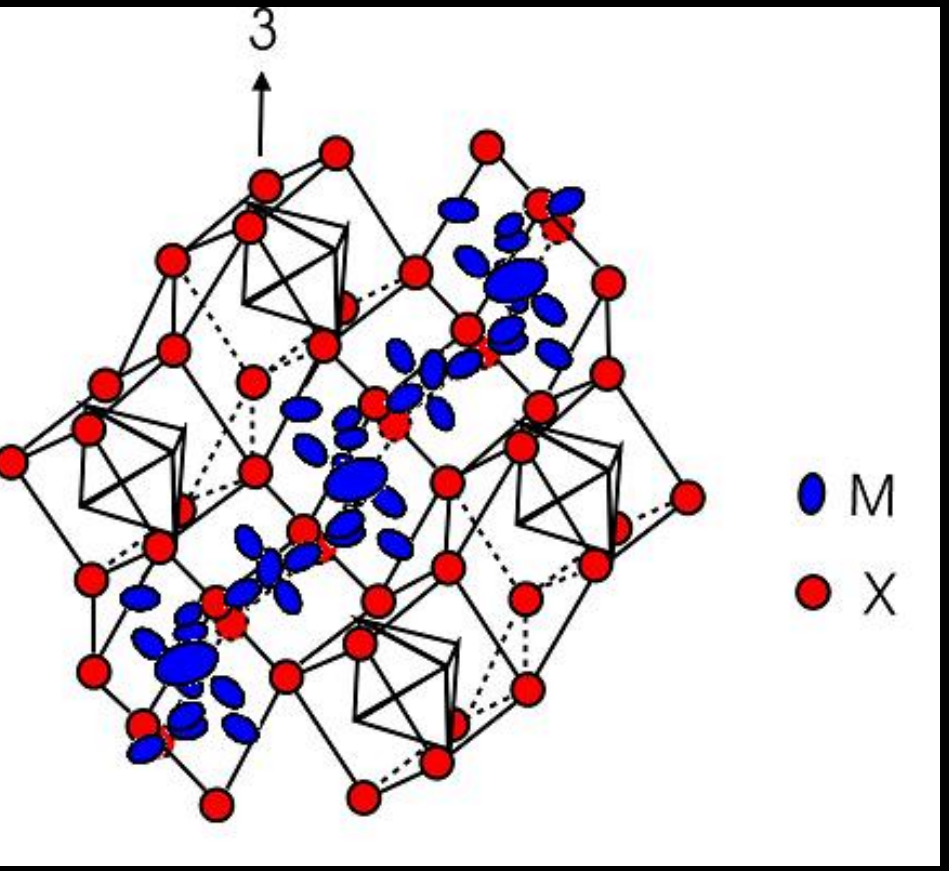

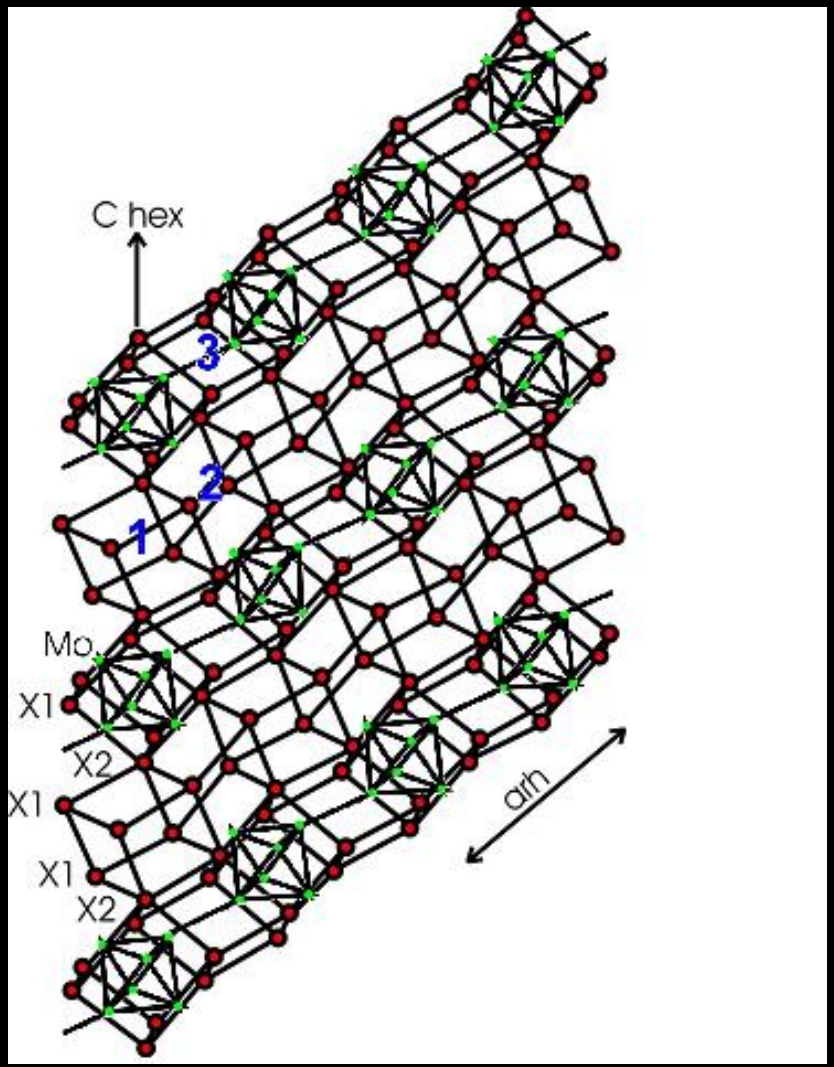

Real samples: $Ti_xMo_6Se_{8-y}$, $Sn_xMo_6Se_{8-y}$ defects not only in M network but also in Se sublattice

Search for Chevrel phases as thermoelectrics (2)

Band structure calculations:

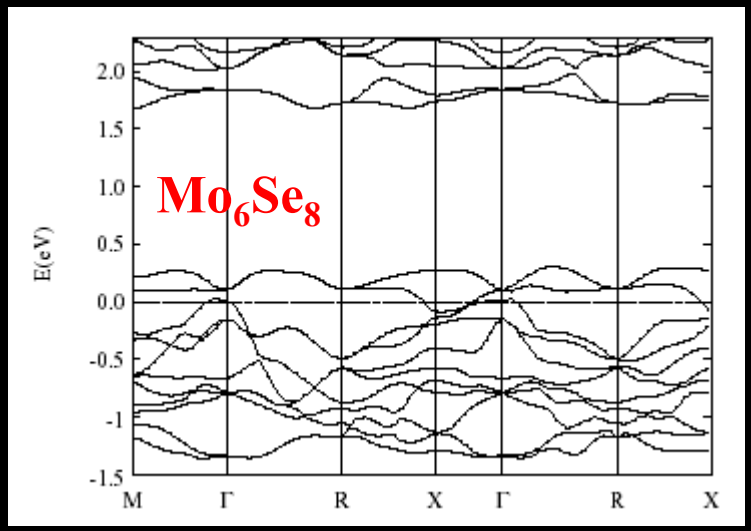

Singh et al. (1999) FP-LAPW

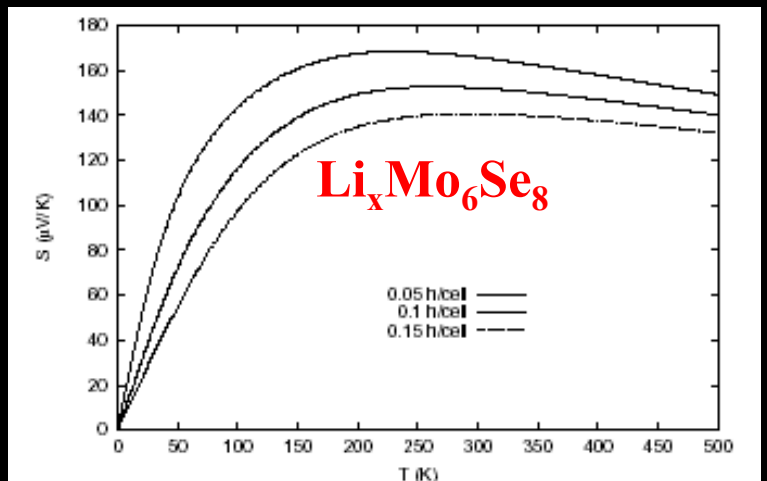

$Zn_2Mo_6Se_8$ (narrow gap E_g<0.1 eV

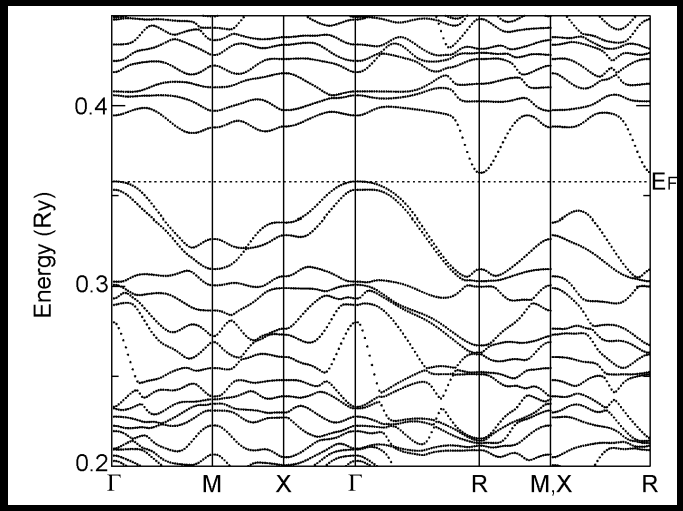

Tobola et al. (1999) KKR

Effective masses

m_e= 0.2 m_o

m_h = 1.2 m_o

$$(M)^{-1}_{ij} = \frac{\partial^2 E}{\partial k_i \partial k_j}$$

Search for Chevrel phases as thermoelectrics

Band structure calculations:

Roche et al. (1998) TB-LMTO; Roche et al. (1999) KKR

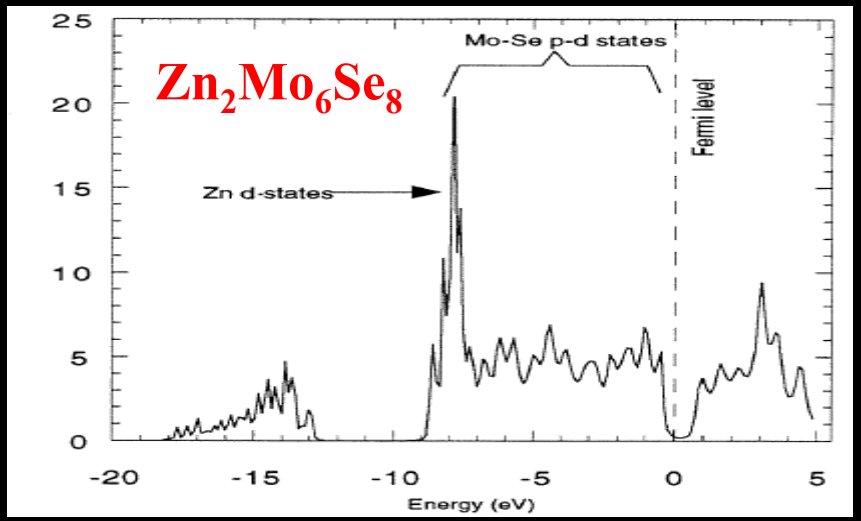

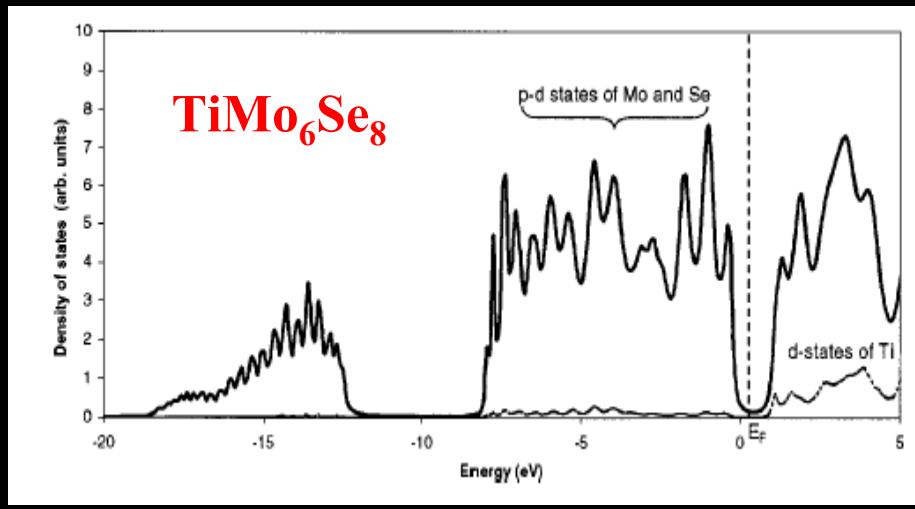

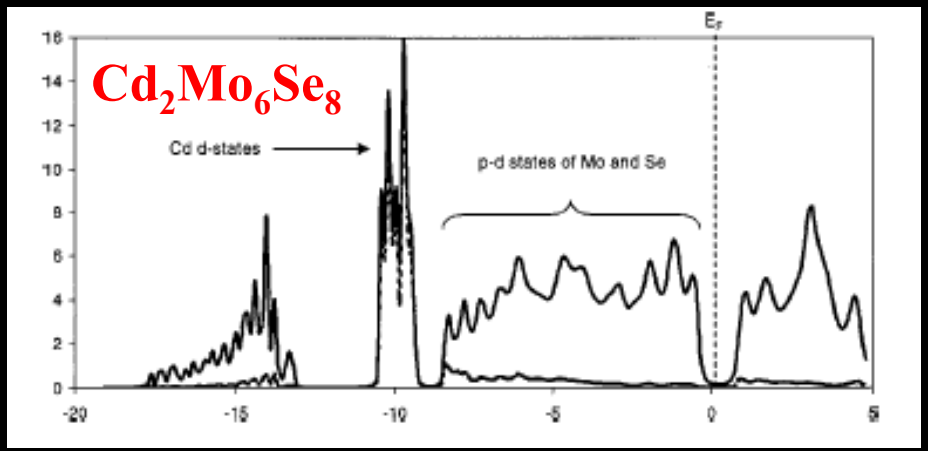

Resistivity experiments

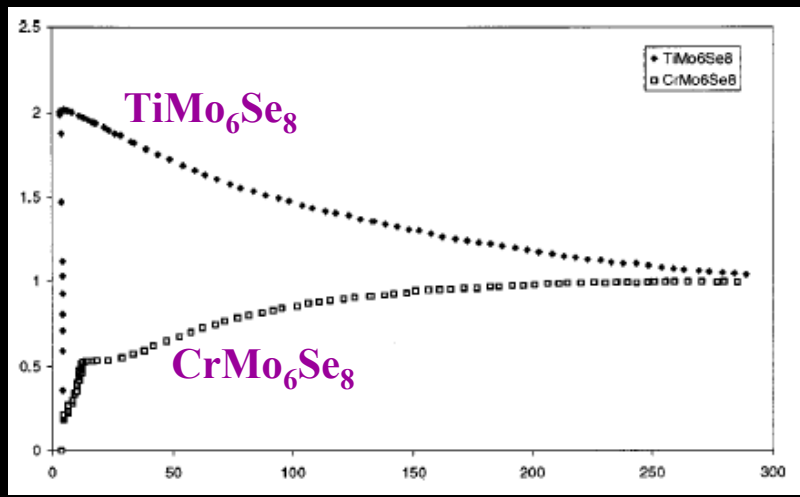

Skutterudites: $CoSb_3$

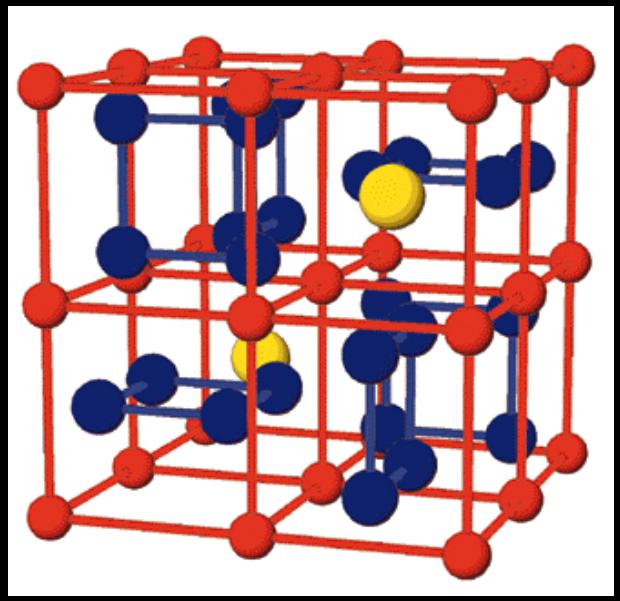

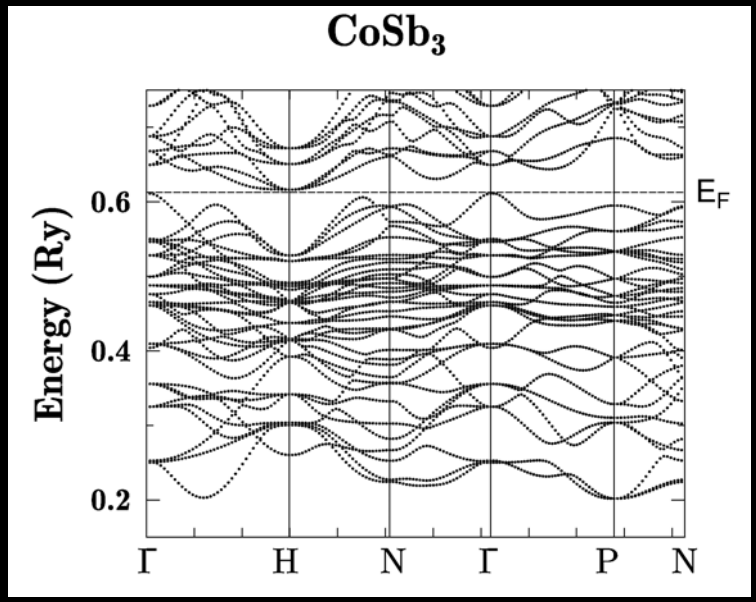

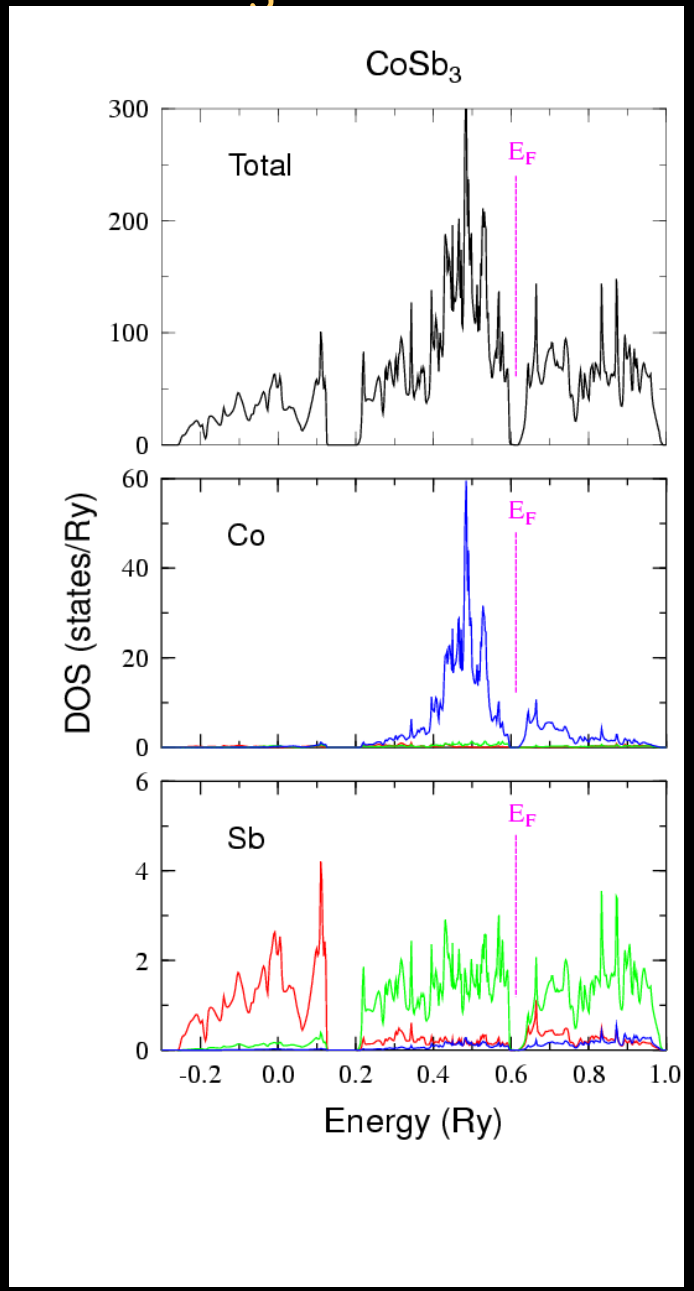

Defects in half-Heusler FeVSb

Jodin, Tobola, … Phys. Rev. B (2004)

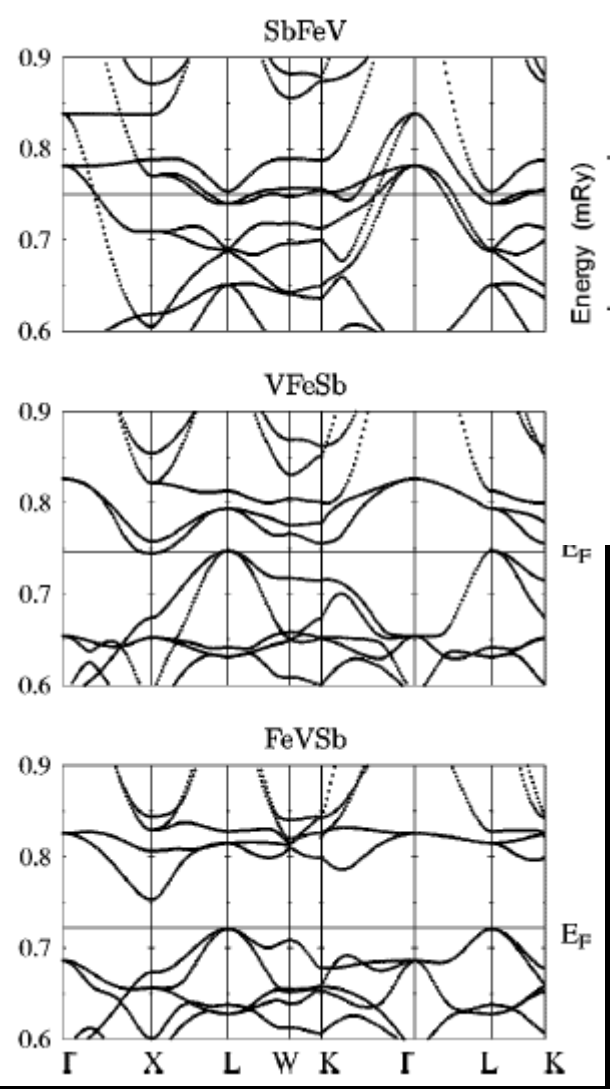

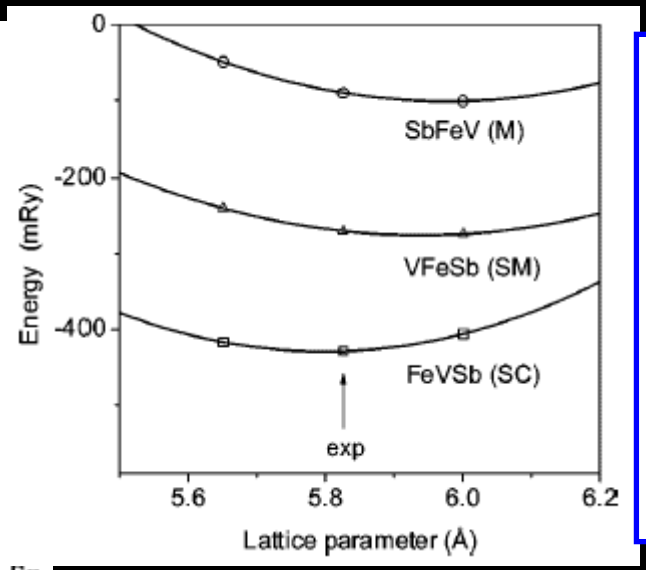

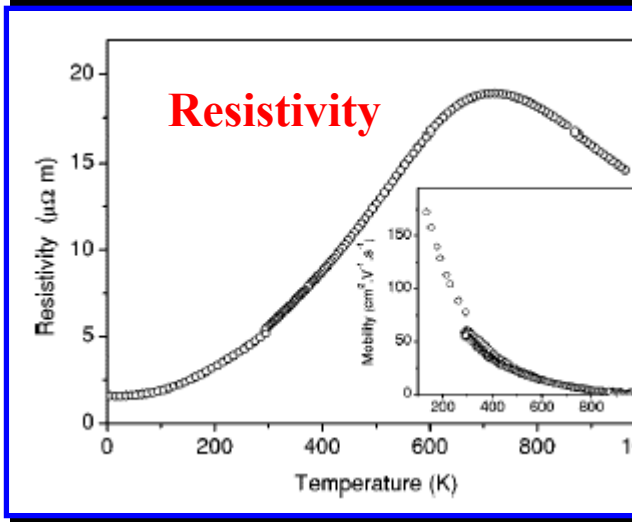

KKR-CPA total energy

Defects: possible origin Of theory-experiment disagreement

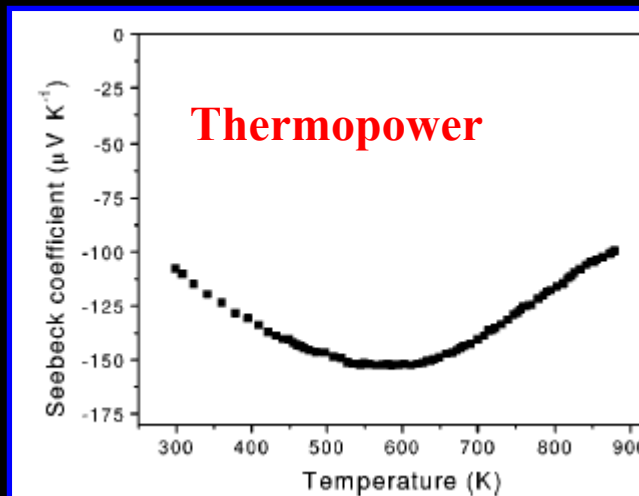

Defects in half-Heusler systems

Nominal	EMPA
FeVSb	$Fe_{0.98}V_{0.99}Sb_{1.03}$
$Fe_{0.995}Co_{0.005}VSb$	$Fe_{0.97}Co_{0.006}V_{0.99}Sb_{1.03}$
$Fe_{0.98}Co_{0.02}VSb$	$Fe_{0.95}Co_{0.02}V_{1.02}Sb_{1.01}$
$FeV_{0.90}Ti_{0.10}Sb$	$Fe_{0.96}V_{0.9}Ti_{0.1}Sb_{1.04}$
$FeV_{0.85}Ti_{0.15}Sb$	$Fe_{0.98}V_{0.86}Ti_{0.15}Sb_{1.01}$
$FeV_{0.80}Ti_{0.20}Sb$	$Fe_{0.99}V_{0.77}Ti_{0.22}Sb_{1.02}$
$FeV_{0.95}Zr_{0.05}Sb$	$Fe_{0.95}V_{0.98}Zr_{0.02}Sb_{1.05}$
$FeV_{0.90}Zr_{0.10}Sb$	$Fe_{0.96}V_{0.97}Zr_{0.03}Sb_{1.04}$
$FeV_{0.85}Zr_{0.15}Sb$	$Fe_{0.95}V_{0.93}Zr_{0.07}Sb_{1.05}$

EPMA data

Jodin, Tobola, … Phys. Rev. B (2004)

KKR-CPA density of states upon inclusion Fe/Sb vac/Fe defects

Vac on Fe and Sb on Fe behave as hole donors

n-type and p-type doping

TABLE IV. Room temperature Seebeck coefficient S and resistivity ρ in pure and substituted FeVSb half-Heusler phases.

Composition	ρ ($\mu\Omega$ m)	S (μV K^{-1})	$n\times10^{20}$(cm^{-3})
FeVSb	5.1	−110	≈1
$Fe_{0.995}Co_{0.005}VSb$	4.2	−130	≈1
$Fe_{0.98}Co_{0.02}VSb$	2.3	−80	≈5
$FeV_{0.95}Ti_{0.05}Sb$	13	+180	≈5
$FeV_{0.90}Ti_{0.10}Sb$	15.5	+145	≈5
$FeV_{0.85}Ti_{0.15}Sb$	68.7	+125	≈2
$FeV_{0.80}Ti_{0.20}Sb$	20	+70	≈20
$FeV_{0.95}Zr_{0.02}Sb$	46	−20	≈1
$FeV_{0.90}Zr_{0.03}Sb$	43	+20	≈3
$FeV_{0.85}Zr_{0.07}Sb$	23	+30	≈4

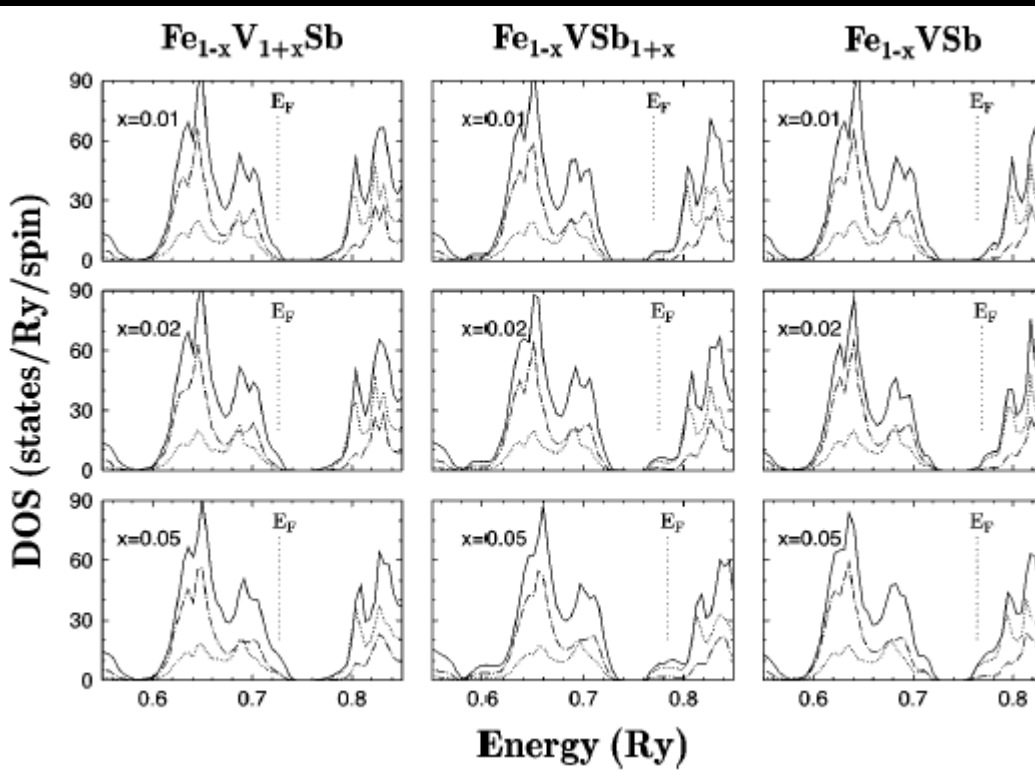

Współpraca

S. Kaprzyk, T. Stopa, B. Wiendlocha
Faculty of Physics and Applied Computer Science
AGH, Kraków, Poland

A. Bansil
Northeastern University, Boston , USA

L. Chaput, L. Jodin P. Pecheur, H. Scherrer,
LPM Ecole des Mines, Nancy

D. Fruchart, J. Pierre
Laboratoire Cristallographie, L. Neel CNRS, Grenoble

B. Malaman, T. Mazet, G. Venturini, A. Verniere
LCSM Université H. Poincaré, Nancy